Deregulation of the endogenous C/EBP{beta} LIP isoform predisposes to tumorigenesis

Begay, V., Smink, J.J., Loddenkemper, C., Zimmermann, K., Rudolph, C., Scheller, M., Steinemann, D., Leser, U., Schlegelberger, B., Stein, H., Leutz, A.

Publication
2015 JAN ; 93(1): 39-49

The final publication is available at Springer via http://dx.doi.org/10.1007/s00109-014-1215-5

Springer Verlag

Deregulation of the endogenous C/EBPβ LIP isoform predisposes to tumorigenesis

Valérie Bégay, Jeske J Smink, Christoph Loddenkemper, Karin Zimmermann, Cornelia Rudolph, Marina Scheller, Doris Steinemann, Ulf Leser, Brigitte Schlegelberger, Harald Stein and Achim Leutz

Affiliations:
V. Bégay, JJ. Smink, M. Scheller
Max Delbrueck Center for Molecular Medicine, Berlin, Germany;
C. Loddenkemper, H. Stein
Charité-Universitätmedizin Berlin, Department of Pathology, Campus Benjamin Franklin, Berlin, Germany;
K. Zimmermann, U. Leser
Institute for Computer Science, Berlin, Humboldt-University of Berlin, Berlin, Germany;
C. Rudolph, D. Steinemann, B. Schlegelberger
Institute of Cell and Molecular Pathology, Hannover Medical School, Hannover, Germany;
A. Leutz
Max Delbrueck Center for Molecular Medicine, Berlin, Germany; Humboldt-University of Berlin, Institute of Biology, [6]Brandenburg Center for Regenerative Therapies, Berlin, Germany.

Corresponding author: Achim Leutz, Univ.-Prof. Dr. rer. nat., Max Delbrueck Center for Molecular Medicine, Dept of Tumorigenesis and Cell Differentiation, Robert-Roessle-Str.10, 13125 BERLIN Germany. Phone: + 49 30 9406 3735, Fax: + 49 30 9406 3298, Email: aleutz@mdc-berlin.de

Keywords: tumorigenesis, lymphomagenesis, translational control, tumor-stroma interaction

Abstract

Two long and one truncated isoforms (termed LAP*, LAP, and LIP, respectively) of the transcription factor C/EBPβ are expressed from a single intronless *Cebpb* gene by alternative translation initiation. Isoform expression is sensitive to mTOR mediated activation of the translation initiation machinery and relayed through an uORF on the C/EBPβ mRNA. The truncated C/EBPβ LIP, initiated by high mTOR activity, has been implied in neoplasia, but it was never shown whether endogenous C/EBPβ LIP may function as an oncogene. In this study we examined spontaneous tumor formation in C/EBPβ knockin mice that constitutively express only the C/EBPβ LIP isoform from its own locus. Our data show that deregulated C/EBPβ LIP predisposes to oncogenesis in many tissues. Gene expression profiling suggests that C/EBPβ LIP supports a pro-tumorigenic microenvironment, resistance to apoptosis, and alteration of cytokine/chemokine expression. The results imply that enhanced translation re-initiation of C/EBPβ LIP promotes tumorigenesis. Accordingly, pharmacological restriction of mTOR function might be a therapeutic option in tumorigenesis that involves enhanced expression of the truncated C/EBPβ LIP isoform.

Introduction

The C/EBPβ transcription factor belongs to the basic leucine zipper (bZip) CCAAT enhancer binding protein (C/EBP) family and controls cell fate in many tissues. C/EBPβ is involved in cell growth, proliferation, differentiation, apoptosis, senescence, and tumor tolerance. *Cebpb* is a single exon gene, yet three isoform proteins of variable N-terminal length are expressed from internal AUG start sites. The two long isoforms (C/EBPβ LAP* and LAP) are both transcriptional activators, but differ by 21 N-terminal amino acid residues that entail chromatin regulatory capacity. The truncated C/EBPβ LIP isoform lacks the N-terminal 185 amino acid residues, removing the entire transactivation domain and part of the regulatory domain. C/EBPβ LIP is thought to dominantly counteract tumor suppressive functions of other C/EBP family members, suggesting C/EBPβ LIP as a potential oncogene [1, 2].

A highly conserved (from fish to man) small upstream open reading frame (uORF) in the 5' mRNA region regulates alternative translation initiation of *Cebpb* at consecutive in frame start sites. Previous data showed that translation of the uORF restrains initiation of C/EBPβ LAP and causes resumption of ribosomal scanning and reinitiation at the downstream C/EBPβ LIP start site. The translational control and C/EBPβ isoform switching depends on mTOR signaling [3-6], stress response pathways [7], and RNA binding-proteins [8]. Briefly, at high activity of the translation initiation machinery the C/EBPβ LIP isoform is preferentially produced, whereas at low activity the long C/EBPβ LAP isoform is preferentially produced [9, 10]. Recent evidences suggested that the C/EBPβ LAP:LIP ratio is an important indicator of C/EBPβ functions. Regulation of C/EBPβ LAP:LIP ratio plays a key role in liver regeneration, acute phase response, bone homeostasis, and mammary gland development [9, 10]. Enhanced expression of C/EBPβ was observed in human tumors, including mammary carcinomas [11-13], anaplastic large cell lymphoma (ALCL) [14-16], endometrial adenocarcinoma [17], ovarian [18], colorectal [19], liver [7] and skin cancer [20]. Among these, enhanced expression of the truncated C/EBPβ LIP isoform was reported in breast, ALCL, ovarian and colorectal neoplasia. C/EBPβ LIP also supports metastasis survival in breast cancer [21] and pharmacological inhibition of C/EBPβ LIP expression reduced ALCL proliferation, implying a causal relationship between C/EBPβ LIP isoform expression and tumorigenesis [14].

Here, we used recombinant mouse genetics to explore whether deregulated expression of C/EBPβ LIP from its own genomic locus supports spontaneous tumor formation. A knockin mouse strain that expresses the C/EBPβ LIP isoform (LIP ki) developed tumors in multiple

tissues of mesenchymal and epithelial origin, providing experimental evidence that enhanced translation re-initiation of C/EBPβ LIP is involved in tumorigenesis.

Materials and Methods

Animals

The generation of C/EBPβ knockout (ko) and LIP ki mice have been previously described [9, 22]. The C/EBPβ ko and LIP ki mice were maintained on a 129 X C57BL/6 genetic background. Mice were fed with standard mouse diet and water ad libitium on a 12-h light-dark cycle. Animals were housed in a pathogen free facility at the Max-Delbrück-Center for Molecular Medicine, Berlin. All procedures and animals experiments were conducted in compliance with protocols approved by the institutional Animal Care and Use Committee. Mice were sacrificed by cervical dislocation. All efforts were made to minimize animal suffering.

Histopathological analyses

Mice were sacrificed upon substantial decline in health (i.e. weight loss, paralysis, ruffling of fur or inactivity) or obvious tumor burden. Tissues were fixed in buffered 4% formaldehyde at 4°C, dehydrated and paraffin embedded. Sections (4μm) were stained with hematoxylin and eosin according to standard procedures. To perform immunohistochemical (IHC) staining slides were immersed in sodium citrate buffer solutions at pH 6.0, heated in a high-pressure cooker for 5 min, rinsed in cold water and washed in Tris-buffered saline (pH 7.4), and were then treated with a peroxidase-blocking reagent (Dako) before incubation for 1 h with the primary antibody for B220 (RA3-6B2, eBioscience) or cleaved-caspase 3 (Asp175, Cell Signaling). Binding was detected by the Envision peroxidase kit (K4010, Dako) using diaminobenzidine as chromogenic substrate. Sections were analyzed using an AxioPlan-2 microscope (Zeiss, Germany). Images were acquired using a Zeiss AxioCam Hr camera and AxioVision software version 4.2. For cleaved-caspase 3 IHC analysis, per animal five randomly chosen microscope fields were captured at 200 x magnification. The number of cleaved-caspase 3 positive cells/field were counted and expressed as fold of control.

Cell culture and immunoblotting

Mouse embryonic fibroblasts (MEFs) were isolated from E13.5 embryos and spontaneously immortalized according to standard protocols. 3T3-L1 murine preadipocytes (ATCC, American Type Culture Collection) and MEFs were cultured in DMEM (Invitrogen) supplemented with 10% FBS (Invitrogen). Tissues, lymphoma and cells were lysed with 8 M urea lysis buffer. Proteins were separated by SDS/PAGE followed by Western blot analysis using rabbit C/EBPβ antibody (C19, Santa Cruz) and mouse anti-α-tubulin (B-7, Santa Cruz)

or mouse anti-β-tubulin (2-28-33, Sigma). Appropriate horseradish peroxidase-conjugated secondary antibodies were used for chemiluminescence (Amersham Biosciences).

RNA preparation and Microarray gene expression profiling

Total RNA from 5 +/L and 5 WT lymphoma was prepared using the TriPure Isolation Reagent (Roche) and analyzed on a 4x44K whole genome mouse microarray (Agilent Technologies). For normalization, quality control, and data analysis, the Bioconductor system was used (http://www.bioconductor.org) [23]. Raw microarray data from Agilent were first quantile normalized. For identification of differentially expressed genes, a linear model was fitted using limma. The fold change cutoff was set to 2 (FC = 2) and the P value cutoff was selected as 0.05. For functional analysis, GSEA was performed using GSEA v2.0 algorithm (http://www.broadinstitute.org/gsea) [24] and the computed t-statistic from limma as pre-ranking. The following gene sets from MSigDB database (http://www.broadinstitute.org/gsea) were used: C2: curated sets, canonical pathways, Biocarta, KEGG, Reactome and C5: Go gene sets, BP: biological process. Only gene sets showing nominal P value ≤ 0.05 and false discovery rate (FDR) ≤ 0.25 were taken into consideration.

Statistical analysis

All data are expressed as mean ± s.e.m. Statistically significant differences between groups were determined using the unpaired two-tailed Mann-Whitney's test for the histographs and the Log-rank test for the Kaplan-Meier curves. Both tests were performed using Prism 5 (GraphPad Software). A P value <0.05 was considered to be statistically significant.

Accession number

The raw microarray data were deposited at Gene Expression Omnibus (GEO accession number: GSE53770)

Results

LIP ki mice are cancer prone

An excess of C/EBPβ LIP has been suggested to promote metastatic breast cancer by interfering with the TGFβ cytostatic pathway and/or by inhibition of anoikis [21, 25]. Moreover, expression of *Cebpb* LIP as a transgene under the whey acidic promoter led to mammary gland hyperplasia and rare neoplasia [26]. Although these experimental approaches have hinted at an oncogenic potential of C/EBPβ LIP, they did not reflect organismal constraints in quantitative, spatial and temporal *Cebpb* regulation from its own locus.

To examine whether enhanced endogenous C/EBPβ LIP expression is involved in tumorigenesis, cohorts of 45 wild type (+/+, WT), 52 C/EBPβ LIP homozygous (L/L) and 72 C/EBPβ LIP heterozygous (+/L) mice were monitored over a period of more than 25 months. Protein analysis confirmed expression of C/EBPβ LIP in the same tissues as C/EBPβ in WT mice (Fig. 1a). Figure 1b illustrates the survival of +/L and L/L mice as compared to their WT siblings. Median survival for WT mice was 24 months, versus 20 months for +/L, and 17 months for L/L mice. These results showed that deregulated expression of the C/EBPβ LIP isoform decreased survival in a dominant and dose-dependent manner.

At 20 months of age, a 3.5-fold increase in tumorigenesis was observed in L/L mice as compared to WT littermates (Table 1 and Fig. 1c). Histopathological analyses of the solid tumors of L/L mice revealed B cell non-Hodgkin lymphoma (B-NHL, 25% in L/L vs 9% in WT), histiocytic sarcoma (HS, 5.8% in L/L vs 0% in WT) and lung adenocarcinoma (1.9% L/L vs 0% in WT) (Table 1 and Fig. S1).

Mice that express one WT *Cebpb* allele and *Cebpb* LIP from the second allele (+/L) reflect translational deregulated, enhanced endogenous C/EBPβ LIP expression. At 20 months of age, 37.5% of the +/L mice had developed solid tumors, in comparison to 9% of the WT mice (Table 1 and Fig. 1c). Compared to L/L mice, the incidence of B-NHL was slightly increased in +/L (32% in +/L vs 25% in L/L), yet the incidence of histiocytic sarcoma and lung adenocarcinoma remained similar (histiocytic sarcoma: 7% in +/L vs 5.8% in L/L; lung adenocarcinoma: 1.4% in +/L vs 1.9% in L/L) (Table 1). A cohort of *Cebpb* heterozygous (*Cebpb* +/-) mice were kept under the same conditions. Median survival was similar in both *Cebpb* +/- and WT littermates (cohort: 25 *Cebpb* +/+ and 27 *Cebpb* +/- mice, median survival: 24 months and 25 months, respectively) and no tumor was found at 20 months of

age (data not shown). Investigation of spontaneous tumor formation in *Cebpb* -/- mice was not possible due to occurrence of infection and severe skin wound phenotype before one year of age in more than 60% of the mice. Altogether our data suggest that increase in C/EBPβ LIP is responsible for tumor development (as in +/L mice) but not a decrease in total C/EBPβ (as in *Cebpb* +/- mice).

B-NHL was found at high incidence in the LIP ki mice. As shown in Figure 1d, LIP ki mice developed B-NHL significantly earlier than WT, although the 129 X C57BL/6 strain is known to be susceptible to B-NHL formation at old age [27]. Interestingly, expression of C/EBPβ, and in particular of the C/EBPβ LIP isoform, is high in lymphoma that develop in WT mice (Fig. 1e), in comparison to the spleens of young WT or LIP ki mice (Fig. 1a) and to the isolated CD19+ B cells (data not shown). Moreover the tumor spectrum in +/L mice was broader than that in L/L mice and included T-lymphoma, carcinoma of the skin, liver, and mammary gland (Table 1, Fig. 2, S2, S3 and S4). Note that C/EBPβ protein expression was detected in all tumor types (Fig. S1, S2 and S5). The generally low carcinoma incidence, however, may be masked by faster lymphoma development, as previously reported in other murine cancer models [28]. These data show that deregulated expression of C/EBPβ LIP from its own locus enhances tumor development in several mesenchymal and epithelial tissues.

Deregulation of cancer pathways in LIP ki mice

To determine which signaling pathways were altered in LIP ki mice tumors, B-NHL tumors obtained from LIP ki and WT mice were examined for cytogenetic alterations using SKY analysis (Table S1). No obvious gross genomic or recurrent rearrangements correlated with enhanced C/EBPβ LIP expression.

Next, gene expression profiling analysis revealed 123 genes as differentially expressed in lymphoma of +/L mice in comparison to lymphoma of WT mice (Fig. 3a and Table S2; 66 upregulated and 57 downregulated genes). Gene set enrichment analysis (GSEA) and examination of leading-edge gene subsets identified enrichment of C2 and C5 functional sets in +/L mice that belong to mTOR pathways (http://www.broadinstitute.org/gsea/msigdb). In addition to mTOR signaling, gene sets involved in translation and regulation of translation, mitochondrial function, metabolism, IGF1, and FOXO pathways, are all significantly enriched in lymphoma of +/L mice (Fig. 3b, c, d, e and Table S3). These data support the notion that elevated C/EBPβ LIP participates in metabolic signaling and mTOR regulated gene expression control during tumorigenesis.

In +/L lymphoma, GSEA highlighted 3 significant gene sets implicated in cell death signaling (Table S3). Moreover, the comparison between lymphoma of WT and +/L mice identified several gene sets involved in MAPkinase, ALK1, TGFβ, and NF-kB pathways that may affect apoptosis and that were significantly depleted in +/L lymphoma (Fig. S6 and Table S3). We also found that the number of apoptotic cells was slightly reduced in the spleen of +/L mice before tumor onset, whereas apoptosis rate was significantly increased in the spleen of *Cebpb* -/- compared to WT mice (Fig. 4a). Furthermore, reduction of caspase 3 cleavage was detected in CD19+ B cells and lymphoma from +/L, as compared to WT (Fig. 4b and 4c, respectively). Similar results were obtained with spleen and CD19+ B cells from L/L mice (data not shown). Altogether these data suggest that increase in C/EBPβ LIP expression reduced the apoptotic rate in B cells and B-NHL.

Deregulation of immune defense might play a key role in tumorigenesis and several previous findings suggested C/EBPβ as an important transcription factor controlling cytokine and chemokine expression in immune cells. Deregulated gene expression comprised known C/EBPβ target genes, including *Saa3*, *S100a9*, *Arg1*, *Fpr1*, *Cxcl13* (Table S2 and [29, 30]). Gene expression profiling showed that approximately 14% of the deregulated genes in +/L lymphoma encoded cytokines/chemokines (Fig. 5a and Table S2). Moreover, the comparison between lymphoma of WT and +/L mice using GSEA revealed leading-edge gene subsets involved in cytokine and chemokine biosynthesis, Toll-like receptor pathways, and innate immune response (Fig. 5b, c, d and Table S3). Expression levels of leukocyte recruiting Ccl3 and Ccl4 cytokines involved in tumor cell eradication, inflammatory M1 type classically activated macrophages (Cxcl13, Cxcl14, Cxcl16, Cx3cr1), and dendritic cells (Cxcl16, Cd11c) markers were all decreased in lymphoma of +/L mice (Fig. 5a). In contrast, M2 activated macrophage markers were enhanced in lymphoma of +/L mice (Fig. 5a; Cd36, Arg1, Ccl24, Mrc1, Retnla, Ccl11, Cd163). These data suggest association of a pro-tumorigenic microenvironment in LIP ki lymphoma.

Collectively, expression profiling and pathway analysis of C/EBPβ LIP lymphoma revealed an increase in pro-tumorigenic cytokine release, deregulation of chemokine expression and TLR signaling pathways, in addition to reduced apoptosis, that may all predispose and contribute to tumor susceptibility. This notion was further supported by recent evidence suggesting C/EBPβ as a critical regulator of myeloid derived suppressor cells that promote the pro-tumorigenic immunosuppressive microenvironment [31].

To test whether deregulated C/EBPβ LIP expression promotes lympho/myelo-proliferation we performed bone marrow (BM) transfer of WT cells into lethally irradiated WT or L/L recipient mice (Fig. S7A). The distribution of hematopoietic cell lineages was different in WT BM reconstituted L/L and WT mice although engraftment of donor cells and the spleen weights were similar in both recipient strains (Fig. S7B and C). An increase in myeloid cells (CD11b positive cells) and a decrease in T cells (CD3 positive cells) were found in the spleens of WT BM reconstituted L/L mice, in comparison to WT BM reconstituted WT mice (B220 positive cells were not affected; Fig. S7D). In peripheral blood, white blood cells (granulocytes, monocytes, lymphocytes) of WT donor origin were higher in L/L than in WT recipient mice (Fig. S7E and F), but no changes in red blood cell counts were observed (Fig. S7G). These data suggest that enhanced expression of the C/EBPβ LIP isoform facilitates a tumor supportive microenvironment, but further experiments are required to determine how the microenvironment is actually altered in LIP mice.

Discussion

Data shown here firmly establish the proto-oncogenic function of endogenous C/EBPβ LIP in mesenchymal and epithelial tissues. Tumors were found in tissues previously shown to depend on C/EBPβ functions, including mammary gland, skin, liver, lung, and hematopoietic cells [15, 16, 30 , 32-34]. Enhanced C/EBPβ LIP expression leads to the development of follicular lymphoma (B-NHL) and histiocytic sarcoma. Human follicular lymphoma may eventually trans-differentiate into histiocytic sarcoma and C/EBPβ was found to be strongly expressed in these tumors [35]. C/EBPβ LIP has also been shown to promote proliferation of human B cell Hodgkin lymphoma and ALCL [14, 16], suggesting an important function of C/EBPβ LIP deregulation in lymphomagenesis and hinting at similarities in disease development in rodents and human.

C/EBPβ LIP is thought to antagonize the long isoforms C/EBPβ LAP*/LAP, other C/EBP members, and some bZIP factors [36, 37]. Accordingly, four scenarios can be envisioned to describe the effect of C/EBPβ LIP on gene expression: (i) C/EBPβ LIP acts alone, (ii) C/EBPβ LIP antagonizes other C/EBP family members or bZIP factors, (iii) C/EBPβ LIP antagonizes the LAP*/LAP isoforms of C/EBPβ or (iv) ii and iii at the same time. C/EBPβ LIP heterozygous mice can reflect all four modes of action while L/L mice can affect (i) and (ii) but not (iii) and (iv). C/EBPβ LIP heterozygous mice develop a broader tumor spectrum and higher percentage of tumor incidence than L/L mice, suggesting that the oncogenic action of C/EBPβ LIP is mediated through antagonism of the C/EBPβ LAP*/LAP isoforms. However, L/L mice die significantly earlier than +/L mice and tumor types that might develop later in life (e.g. requiring more oncogenic events) will not be found in L/L mice. Similarly, analysis of spontaneous tumor formation in *p53* deficient mice showed a wider tumor spectrum in *p53* +/- mice as compared to *p53* -/- mice [28]. These data suggests that dosage effects of oncogenes or tumor suppressor genes may affect tumor development. Carcinogen-induced tumorigenesis in LIP ki mice or combination with other murine oncogenic models will help to resolve the underlying molecular events in future experiments. Surprisingly and in contrast to the *Cebpb* -/- mice, L/L and +/L mice both do not show skin phenotypes, loss of hair or reduced fat content (data not shown), suggesting that C/EBPβ LIP isoform functions are not reflecting simple loss of function phenotypes and go beyond inhibition of C/EBPβ LAP*/LAP or other C/EBPs members in the skin or fat. These observations support the notion that regulatory capacity by C/EBPβ LIP is context dependent and more complex that the four possibilities of action, as noted above. Nevertheless, it was important to first analyze spontaneous tumor formation in LIP ki mice

and here, our data revealed the oncogenic potential of C/EBPβ LIP from its own locus in divers tissues.

The long latency of tumor development in LIP ki mice suggests that additional oncogenic events are required in conjunction with C/EBPβ LIP deregulation. Co-operation of several proto-oncogenes and loss of tumor suppressor functions is a common explanation of tumor development. However, tumorigenesis was not accelerated in compound mice heterozygous for p53 deletion and C/EBPβ LIP deregulation, as compared to p53 heterozygous mice (data not shown). It therefore remains to be resolved which additional oncogenic events may accelerate tumor development in +/L or L/L mice.

The GSEA analyses indicated several altered pathways in lymphoma of LIP ki mice that relate to autonomous and non-cell autonomous effects on B cell lymphomagenesis. The structural features of *Cebpb* gene (lack of introns), however, render a conditional genetic approach rather difficult to experimentally resolve how C/EBPβ LIP supports oncogenesis. In contrast to *Cebpa*, no mutational alterations within the *Cebpb* coding region that affect the isoform expression have yet been reported. However, deregulation of C/EBPβ LIP expression may occur on the signaling/proteomic, rather than on the genomic level. In any case, our results show that tight regulation of the balance between long and truncated C/EBPβ isoforms is important for preventing tumor formation. Accordingly, the data imply that translational deregulation may dysbalance C/EBPβ isoform expression to contribute to tumorigenesis.

Previously, we have shown that the mTOR-TORC1 inhibitor rapamycin restricts upregulation of C/EBPβ LIP expression and lymphoma xenograft growth [3, 14]. Moreover, a translational control defective C/EBPβ mutant phenocopied mTOR inhibition and mTOR target genes were found to be co-regulated by C/EBPβ and thus identified C/EBPβ as an important mediator of mTOR functions [9, 10]. Activation of mTOR promotes protein biosynthesis, translation reinitiation, M2 polarization, cell survival, and tumorigenesis, [38, 39]. Deregulated mTOR signaling is evident in lymphomagenesis and leukemogenesis and development of therapeutic strategies based on mTOR inhibition are currently under investigation [40, 41]. Lymphoma cells of C/EBPβ LIP heterozygous mice showed enrichment of rapamycin sensitive genes, including FABP4 and adipokines that are thought to play an important role in tumorigenesis [42]. In addition, eIF-4E, a key factor of translation initiation that is regulated by the mTOR sensitive 4EBPs also up-regulates C/EBPβ LIP expression and promotes neoplasia [3, 43]. Our data therefore imply that pharmacologic

interference with uORF mediated C/EBPβ LIP translation initiation control may help to re-establish the balance between C/EBPβ isoforms and oppose deregulated mTOR signaling.

Acknowledgments

We thank E. Sterneck for providing the *cebpβ* ko mouse strain, HP Rahn for help with flow cytometry, the radiology department of the Helios Klinikum for help with X-ray radiation and C. Becker, J. Bergemann, A.V. Giese, P. Heinrich-Gossen, S. Jaksch, R. Leu, S. Spieckermann and R. Zarmstorff for technical assistance. We are grateful to F. Rosenbauer and T. Müller for valuable discussions. This work was supported by the Deutsche Krebsgesellschaft (grant n° LEFF200708 to A.L) and by the German Research Council (grant n° TRR-54 to A.L. and U.L.).

Disclosure The authors declare no conflict of interest related to this study.

References

1. Wethmar K, Smink JJ, Leutz A (2010) Upstream open reading frames: molecular switches in (patho)physiology. BioEssays : news and reviews in molecular, cellular and developmental biology 32: 885-893
2. Zahnow CA (2009) CCAAT/enhancer-binding protein beta: its role in breast cancer and associations with receptor tyrosine kinases. Expert Rev Mol Med 11: e12
3. Calkhoven CF, Muller C, Leutz A (2000) Translational control of C/EBPalpha and C/EBPbeta isoform expression. Genes Dev 14: 1920-1932
4. Nardella C, Carracedo A, Salmena L, Pandolfi PP (2010) Faithfull modeling of PTEN loss driven diseases in the mouse. Curr Top Microbiol Immunol 347: 135-168
5. Ossipow V, Descombes P, Schibler U (1993) CCAAT/enhancer-binding protein mRNA is translated into multiple proteins with different transcription activation potentials. Proc Natl Acad Sci U S A 90: 8219-8223
6. Zoncu R, Efeyan A, Sabatini DM (2011) mTOR: from growth signal integration to cancer, diabetes and ageing. Nat Rev Mol Cell Biol 12: 21-35
7. Li Y, Bevilacqua E, Chiribau CB, Majumder M, Wang C, Croniger CM, Snider MD, Johnson PF, Hatzoglou M (2008) Differential control of the CCAAT/enhancer-binding protein beta (C/EBPbeta) products liver-enriched transcriptional activating protein (LAP) and liver-enriched transcriptional inhibitory protein (LIP) and the regulation of gene expression during the response to endoplasmic reticulum stress. J Biol Chem 283: 22443-22456. DOI 10.1074/jbc.M801046200
8. Timchenko NA, Wang GL, Timchenko LT (2005) RNA CUG-binding protein 1 increases translation of 20-kDa isoform of CCAAT/enhancer-binding protein beta by interacting with the alpha and beta subunits of eukaryotic initiation translation factor 2. J Biol Chem 280: 20549-20557. DOI 10.1074/jbc.M409563200
9. Smink JJ, Begay V, Schoenmaker T, Sterneck E, de Vries TJ, Leutz A (2009) Transcription factor C/EBPbeta isoform ratio regulates osteoclastogenesis through MafB. Embo J 28: 1769-1781
10. Wethmar K, Begay V, Smink JJ, Zaragoza K, Wiesenthal V, Dorken B, Calkhoven CF, Leutz A (2010) C/EBPbetaDeltauORF mice--a genetic model for uORF-mediated translational control in mammals. Genes Dev 24: 15-20
11. Dearth LR, Hutt J, Sattler A, Gigliotti A, DeWille J (2001) Expression and function of CCAAT/enhancer binding proteinbeta (C/EBPbeta) LAP and LIP isoforms in mouse mammary gland, tumors and cultured mammary epithelial cells. J Cell Biochem 82: 357-370
12. Milde-Langosch K, Loning T, Bamberger AM (2003) Expression of the CCAAT/enhancer-binding proteins C/EBPalpha, C/EBPbeta and C/EBPdelta in breast cancer: correlations with clinicopathologic parameters and cell-cycle regulatory proteins. Breast Cancer Res Treat 79: 175-185
13. Zahnow CA, Younes P, Laucirica R, Rosen JM (1997) Overexpression of C/EBPbeta-LIP, a naturally occurring, dominant-negative transcription factor, in human breast cancer. J Natl Cancer Inst 89: 1887-1891
14. Jundt F, Raetzel N, Muller C, Calkhoven CF, Kley K, Mathas S, Lietz A, Leutz A, Dorken B (2005) A rapamycin derivative (everolimus) controls proliferation through down-regulation of truncated CCAAT enhancer binding protein {beta} and NF-{kappa}B activity in Hodgkin and anaplastic large cell lymphomas. Blood 106: 1801-1807
15. Piva R, Pellegrino E, Mattioli M, Agnelli L, Lombardi L, Boccalatte F, Costa G, Ruggeri BA, Cheng M, Chiarle R, Palestro G, Neri A, Inghirami G (2006) Functional validation of the anaplastic lymphoma kinase signature identifies CEBPB and BCL2A1 as critical target genes. J Clin Invest 116: 3171-3182
16. Quintanilla-Martinez L, Pittaluga S, Miething C, Klier M, Rudelius M, Davies-Hill T, Anastasov N, Martinez A, Vivero A, Duyster J, Jaffe ES, Fend F, Raffeld M (2006) NPM-ALK-dependent expression of the transcription factor CCAAT/enhancer binding protein beta

in ALK-positive anaplastic large cell lymphoma. Blood 108: 2029-2036. DOI blood-2005-10-014258 [pii]
10.1182/blood-2005-10-014258
17. Arnett B, Soisson P, Ducatman BS, Zhang P (2003) Expression of CAAT enhancer binding protein beta (C/EBP beta) in cervix and endometrium. Mol Cancer 2: 21
18. Sundfeldt K, Ivarsson K, Carlsson M, Enerback S, Janson PO, Brannstrom M, Hedin L (1999) The expression of CCAAT/enhancer binding protein (C/EBP) in the human ovary in vivo: specific increase in C/EBPbeta during epithelial tumour progression. Br J Cancer 79: 1240-1248
19. Rask K, Thorn M, Ponten F, Kraaz W, Sundfeldt K, Hedin L, Enerback S (2000) Increased expression of the transcription factors CCAAT-enhancer binding protein-beta (C/EBBeta) and C/EBzeta (CHOP) correlate with invasiveness of human colorectal cancer. Int J Cancer 86: 337-343
20. Oh HS, Smart RC (1998) Expression of CCAAT/enhancer binding proteins (C/EBP) is associated with squamous differentiation in epidermis and isolated primary keratinocytes and is altered in skin neoplasms. J Invest Dermatol 110: 939-945
21. Gomis RR, Alarcon C, Nadal C, Van Poznak C, Massague J (2006) C/EBPbeta at the core of the TGFbeta cytostatic response and its evasion in metastatic breast cancer cells. Cancer Cell 10: 203-214
22. Sterneck E, Tessarollo L, Johnson PF (1997) An essential role for C/EBPbeta in female reproduction. Genes Dev 11: 2153-2162
23. Gentleman RC, Carey VJ, Bates DM, Bolstad B, Dettling M, Dudoit S, Ellis B, Gautier L, Ge Y, Gentry J, Hornik K, Hothorn T, Huber W, Iacus S, Irizarry R, Leisch F, Li C, Maechler M, Rossini AJ, Sawitzki G, Smith C, Smyth G, Tierney L, Yang JY, Zhang J (2004) Bioconductor: open software development for computational biology and bioinformatics. Genome biology 5: R80. DOI 10.1186/gb-2004-5-10-r80
24. Subramanian A, Tamayo P, Mootha VK, Mukherjee S, Ebert BL, Gillette MA, Paulovich A, Pomeroy SL, Golub TR, Lander ES, Mesirov JP (2005) Gene set enrichment analysis: a knowledge-based approach for interpreting genome-wide expression profiles. Proc Natl Acad Sci U S A 102: 15545-15550. DOI 10.1073/pnas.0506580102
25. Li H, Baldwin BR, Zahnow CA (2011) LIP expression is regulated by IGF-1R signaling and participates in suppression of anoikis. Mol Cancer 10: 100. DOI 10.1186/1476-4598-10-100
26. Zahnow CA, Cardiff RD, Laucirica R, Medina D, Rosen JM (2001) A role for CCAAT/enhancer binding protein beta-liver-enriched inhibitory protein in mammary epithelial cell proliferation. Cancer Res 61: 261-269
27. Ward JM (2006) Lymphomas and leukemias in mice. Exp Toxicol Pathol 57: 377-381. DOI S0940-2993(06)00041-8 [pii]
10.1016/j.etp.2006.01.007
28. Harvey M, McArthur MJ, Montgomery CA, Jr., Butel JS, Bradley A, Donehower LA (1993) Spontaneous and carcinogen-induced tumorigenesis in p53-deficient mice. Nat Genet 5: 225-229
29. Bonzheim I, Irmler M, Klier-Richter M, Steinhilber J, Anastasov N, Schafer S, Adam P, Beckers J, Raffeld M, Fend F, Quintanilla-Martinez L (2013) Identification of C/EBPbeta Target Genes in ALK+ Anaplastic Large Cell Lymphoma (ALCL) by Gene Expression Profiling and Chromatin Immunoprecipitation. PLoS One 8: e64544. DOI 10.1371/journal.pone.0064544
30. Uematsu S, Kaisho T, Tanaka T, Matsumoto M, Yamakami M, Omori H, Yamamoto M, Yoshimori T, Akira S (2007) The C/EBP beta isoform 34-kDa LAP is responsible for NF-IL-6-mediated gene induction in activated macrophages, but is not essential for intracellular bacteria killing. J Immunol 179: 5378-5386
31. Marigo I, Bosio E, Solito S, Mesa C, Fernandez A, Dolcetti L, Ugel S, Sonda N, Bicciato S, Falisi E, Calabrese F, Basso G, Zanovello P, Cozzi E, Mandruzzato S, Bronte V (2010) Tumor-induced tolerance and immune suppression depend on the C/EBPbeta transcription factor. Immunity 32: 790-802. DOI 10.1016/j.immuni.2010.05.010

32. Nerlov C (2007) The C/EBP family of transcription factors: a paradigm for interaction between gene expression and proliferation control. Trends in cell biology 17: 318-324. DOI 10.1016/j.tcb.2007.07.004
33. Nerlov C (2010) Transcriptional and translational control of C/EBPs: the case for "deep" genetics to understand physiological function. BioEssays : news and reviews in molecular, cellular and developmental biology 32: 680-686. DOI 10.1002/bies.201000004
34. Ramji DP, Foka P (2002) CCAAT/enhancer-binding proteins: structure, function and regulation. The Biochemical journal 365: 561-575. DOI 10.1042/BJ20020508
35. Feldman AL, Arber DA, Pittaluga S, Martinez A, Burke JS, Raffeld M, Camos M, Warnke R, Jaffe ES (2008) Clonally related follicular lymphomas and histiocytic/dendritic cell sarcomas: evidence for transdifferentiation of the follicular lymphoma clone. Blood 111: 5433-5439
36. Newman JR, Keating AE (2003) Comprehensive identification of human bZIP interactions with coiled-coil arrays. Science 300: 2097-2101. DOI 10.1126/science.1084648
37. Vinson C, Myakishev M, Acharya A, Mir AA, Moll JR, Bonovich M (2002) Classification of human B-ZIP proteins based on dimerization properties. Molecular and cellular biology 22: 6321-6335
38. Chen W, Ma T, Shen XN, Xia XF, Xu GD, Bai XL, Liang TB (2012) Macrophage-induced tumor angiogenesis is regulated by the TSC2-mTOR pathway. Cancer Res 72: 1363-1372. DOI 10.1158/0008-5472.CAN-11-2684
39. Menon S, Yecies JL, Zhang HH, Howell JJ, Nicholatos J, Harputlugil E, Bronson RT, Kwiatkowski DJ, Manning BD (2012) Chronic activation of mTOR complex 1 is sufficient to cause hepatocellular carcinoma in mice. Science signaling 5: ra24. DOI 10.1126/scisignal.2002739
40. Chiarini F, Evangelisti C, Buontempo F, Bressanin D, Fini M, Cocco L, Cappellini A, McCubrey JA, Martelli AM (2012) Dual Inhibition of Phosphatidylinositol 3-Kinase and Mammalian Target of Rapamycin: a Therapeutic Strategy for Acute Leukemias. Current cancer drug targets
41. Xu ZZ, Xia ZG, Wang AH, Wang WF, Liu ZY, Chen LY, Li JM (2013) Activation of the PI3K/AKT/mTOR pathway in diffuse large B cell lymphoma: clinical significance and inhibitory effect of rituximab. Annals of hematology 92: 1351-1358. DOI 10.1007/s00277-013-1770-9
42. Lee D, Wada K, Taniguchi Y, Al-Shareef H, Masuda T, Usami Y, Aikawa T, Okura M, Kamisaki Y, Kogo M (2014) Expression of fatty acid binding protein 4 is involved in the cell growth of oral squamous cell carcinoma. Oncology reports 31: 1116-1120. DOI 10.3892/or.2014.2975
43. Ruggero D, Montanaro L, Ma L, Xu W, Londei P, Cordon-Cardo C, Pandolfi PP (2004) The translation factor eIF-4E promotes tumor formation and cooperates with c-Myc in lymphomagenesis. Nature medicine 10: 484-486. DOI 10.1038/nm1042

Figure legends

Fig. 1 LIP ki mice are cancer prone. (**a**). C/EBPβ isoform expression in tissues of WT and LIP ki mice. Various tissues isolated from 8-week-old WT and LIP ki mice (+/L, L/L) were lysed in 8 M urea lysis buffer and analyzed by Western blotting for expression of C/EBPβ isoforms LAP*, LAP and LIP (as indicated). M.GL.: mammary gland; WAT: white adipose tissue; BAT: brown adipose tissue; Pan: pancreas; BM: bone marrow. 3T3-L1 cells (L1) and C/EBPα -/- MEF ($\alpha^{-/-}$) were used as positive controls whereas C/EBPβ -/- MEF ($\beta^{-/-}$) were used as negative controls. α-tubulin was used as internal control. White asterisk (*): unspecific immune reactivity. (**b**) Dosage effect of C/EBPβ LIP on survival rate. Kaplan-Meier curve of +/+ (black line) and LIP ki mice (+/L, orange line; L/L, green line) housed over a period of 25 months. Mice were monitored twice weekly for tumor formation. Moribund mice or mice showing fatal illness or tumor development were sacrificed and tissues were isolated for further examination. Cohorts of mice: +/+ n= 45; +/L n = 72; L/L n = 52. Accelerated death of +/L and L/L mice versus +/+ mice, and of +/L mice versus L/L mice according to the Log-rank test was significant in each case: ***P< 0.0001. (**c**) Comparison of survival rate and tumor incidence at 20 months of age between LIP ki mutants and WT mice: +/+ (4 tumors out 45 +/+ mice); +/L (27 tumors out of 72 mice); L/L (16 tumors out of 52 mice). (**d**) Comparison of average age for lymphoma development in WT and LIP ki mice. Cohorts of mice: +/+ n= 45; +/L n = 72; L/L n = 52. Error bars show SEM. Significant accelerated lymphoma development of +/L and L/L mice versus +/+ mice were analyzed using the unpaired two-tailed Mann-Whitney's test: ***P< 0.0001. (**e**) Lymphoma found in WT and LIP ki mice were lysed in 8 M urea lysis buffer and analyzed by Western blotting for expression of C/EBPβ isoforms LAP*, LAP and LIP (as indicated). β-tubulin was used as internal control.

Fig. 2 LIP ki mice develop mesenchymal and epithelial tumors. Histological analysis (H&E staining) of mesenchymal (**a** and **c**) and epithelial (**d**-**h**) tumors found in the +/L mice. (**a**-**b**) B cell non-hodgkin lymphoma (B-NHL, **a**) with massive infiltration of B cells in the liver (arrows in **a**) characterized by B220 immunopositive staining (arrows in **b**). See Fig. S1 for further characterization of the B-NHL. (**c**) A histiocytic sarcoma with nodular infiltrates (arrows) developed in the spleen. See Fig. S2 for further characterization of the histiocytic sarcoma. (**d**) Liver with a hepatocellular carcinoma (HCC) showing a trabecular growth pattern (arrow). Arrowhead: mitotic figure. (**e**-**f**) A ductal (**e**) and a tubular (**f**) mammary carcinoma developed in a +/L female of 16 months of age. (**g**) Skin carcinoma with squamous differentiation and keratinization (arrowhead) as well as horn pearl formation (arrow). (**h**) Lung adenocarcinoma with papillary growth pattern. **a**, **b**: scale bar = 25 μm; **c**, **d**, **g**, **h**: scale

bar = 20 µm; **e**, **f**: scale bar = 10 µm. See Fig S3 and S4 for comparison with non-tumor tissues from age-matched +/+ mice.

Fig. 3 Gene expression profiling analysis of B-NHL of LIP ki mice. (**a**) Heat map of differentially regulated genes in B-NHL of +/L mice in comparison to B-NHL of WT mice as identified by gene array analysis. +/+ n = 5; +/L n = 5, See list of the genes in Table S2. (**b-e**) GSEA based on the comparison of B-NHL of +/L and WT mice for enrichment or depletion of rapamycin sensitive genes (**b**), translation (**c**), FOXO pathway (**d**) and oxidative phosphorylation and TCA cycle and respiratory electron transport (**e**) associated genes. The normalized enrichment scores (NES) and P values are indicated in each plot. Note the positive NES values observed in all cases indicating an upregulation of these gene sets in B-NHL of +/L mice compared to B-NHL of WT mice.

Fig. 4 Impaired apoptosis in LIP ki mice before and after tumor onset. (**a**)**.** Number of apoptotic cells in the splenic white pulp of C/EBPβ mutants and WT mice before tumor onset. Apoptotic cells were analyzed using cleaved-caspase 3 immunostaining. Numbers of positive cleaved-caspase 3 cells/field were counted and expressed as fold of control. n = 5 per genotype. Error bars show SEM. *P<0.05. (**b-c**)**.** Representative immunoblot analyses showing decrease in cleaved-caspase 3 (Cl.caspase 3) expression in CD19+ B cells sorted from spleen of 12 months-old LIP ki mice as compared with those of WT counterparts (**b**) and in B-NHL of LIP ki mice as compared with B-NHL of WT mice (**c**). β-tubulin was used as loading control. The CD19+ B cells samples were run on the same gel, but were noncontiguous (same for B-NHL samples).

Fig. 5 Deregulated C/EBPβ LIP expression altered cytokines and chemokines expression levels in B-NHL of LIP ki mice. (**a**) Heat map showing deregulated expression of cytokines and chemokines in B-NHL of +/L mice in comparison to B-NHL of WT mice. +/+ n = 5; +/L n = 5. (**b-d**) GSEA based on the comparison of B-NHL of +/L and WT mice for enrichment or depletion of regulation of cytokine biosynthetic process (**b**), Toll like receptor signaling pathway (**c**), and innate immune system (**d**) associated-genes. The normalized enrichment scores (NES) and P values are indicated in each plot. Note the negative NES values observed in all cases indicating a depletion of these gene sets in B-NHL of +/L mice compared to B-NHL of WT mice.

TABLES

Table 1 Tumor distribution in LIP ki mice at 20 months of age.

Genotype	+/+	+/L	L/L
Number dead/cohort	11/45	41/72	44/52[a]
Tumor incidence:			
/cohort	4/45 (9%)	27/72 (37.5%)***	16/52 (30.8%)**
/number dead	4/11 (36%)	27/41 (66%)*	16/44 (36%)
B-NHL	4/45 (9%)	23/72 (32%)	13/52 (25%)
T-lymphoma	0	1/72	0
Histiocytic sarcoma	0	5/72	3/52
Mammary gland carcinoma	0	2/72	0
HCC	0	1/72	0
Skin carcinoma	0	1/72	0
Lung tumor	0	1/72	1/52

Note that some mice developed multiple primary solid tumors. Tumor incidence reflects number of mice with any kind of tumor(s) even though an animal might develop more than one tumor. B-NHL: B non-Hodgkin lymphoma, HCC: hepatocellular carcinoma.
Unpaired t test: *P<0.02; **P<0.005; ***P<0.0005.
[a]L/L mice show a high death rate but a lower tumor incidence in comparison to +/L mice. L/L mice developed more infection and abscess than +/L and +/+ mice.

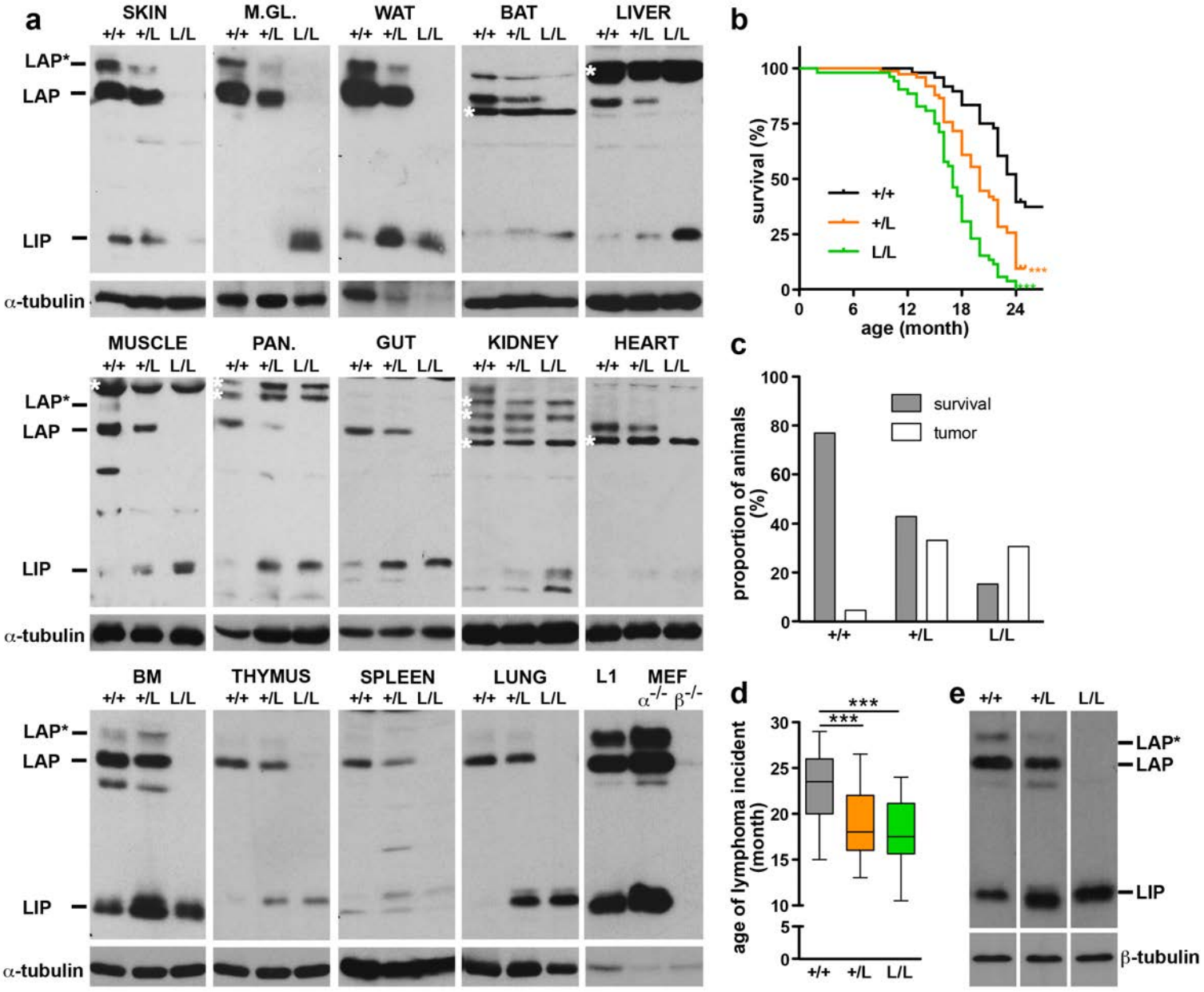
a
SKIN
M.GL.
WAT
BAT
LIVER
+/+ +/L L/L
LAP*
LAP
LIP
α-tubulin
MUSCLE
PAN.
GUT
KIDNEY
HEART
BM
THYMUS
SPLEEN
LUNG
L1
MEF
α-/- β-/-
b
survival (%)
age (month)
+/+
+/L
L/L
***
c
proportion of animals (%)
survival
tumor
d
age of lymphoma incident (month)
***
e
β-tubulin

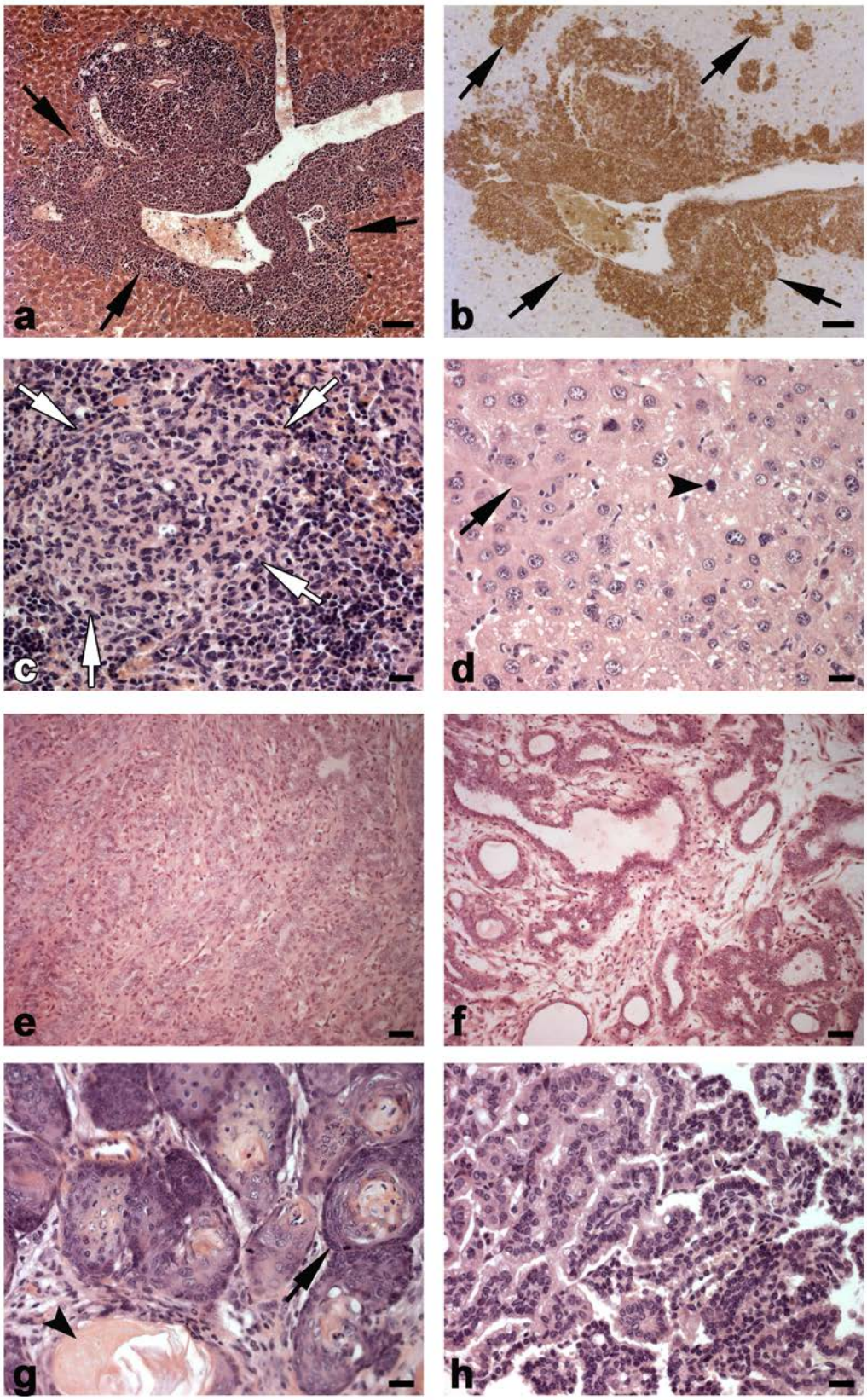
a
b
c
d
e
f
g
h

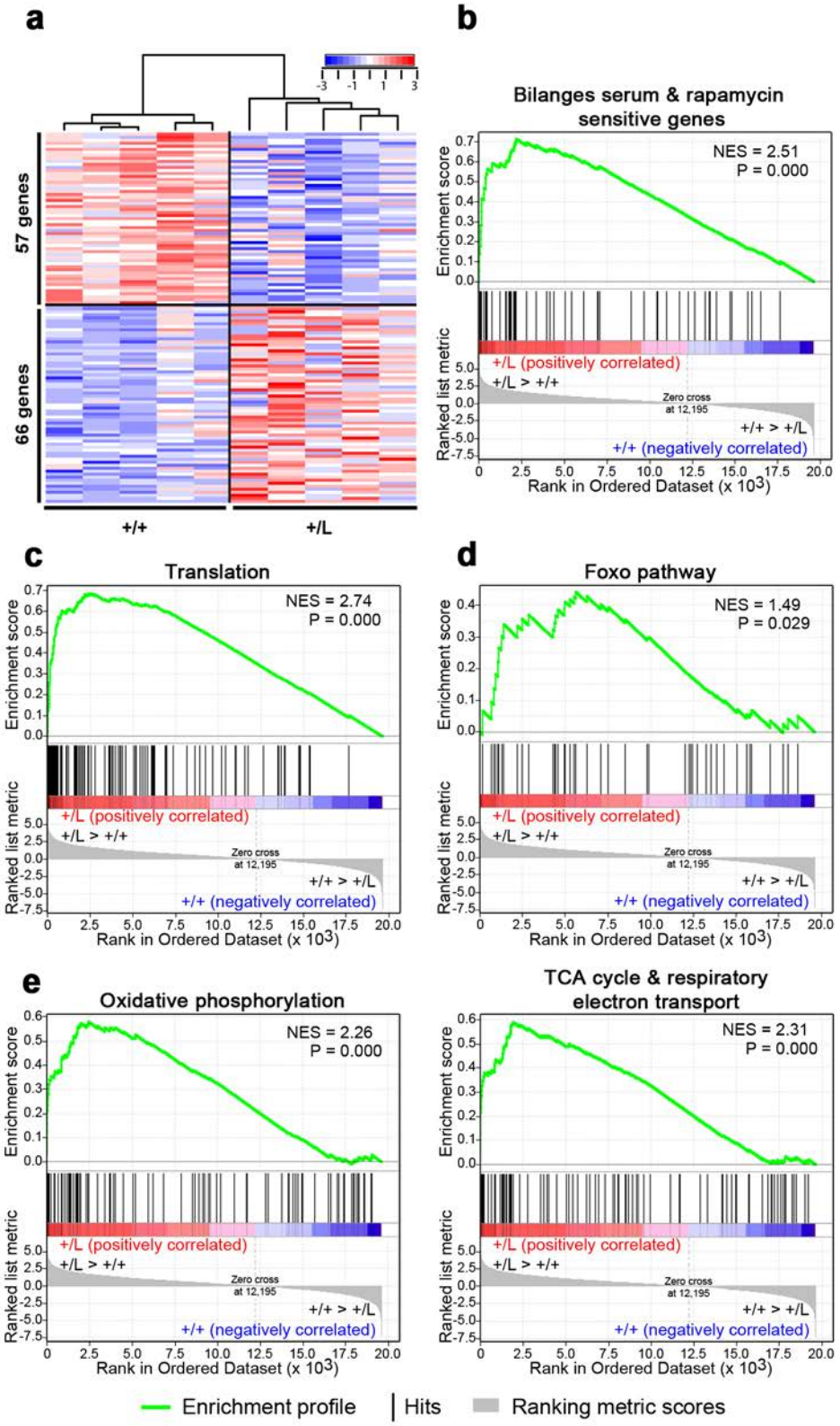
a
-3
-1
1
3
57 genes
66 genes
+/+
+/L
b
Bilanges serum & rapamycin sensitive genes
NES = 2.51
P = 0.000
Enrichment score
Ranked list metric
+/L (positively correlated)
+/L > +/+
Zero cross at 12,195
+/+ > +/L
+/+ (negatively correlated)
Rank in Ordered Dataset (x 10^3)
c
Translation
NES = 2.74
P = 0.000
d
Foxo pathway
NES = 1.49
P = 0.029
e
Oxidative phosphorylation
NES = 2.26
P = 0.000
TCA cycle & respiratory electron transport
NES = 2.31
P = 0.000
Enrichment profile
Hits
Ranking metric scores

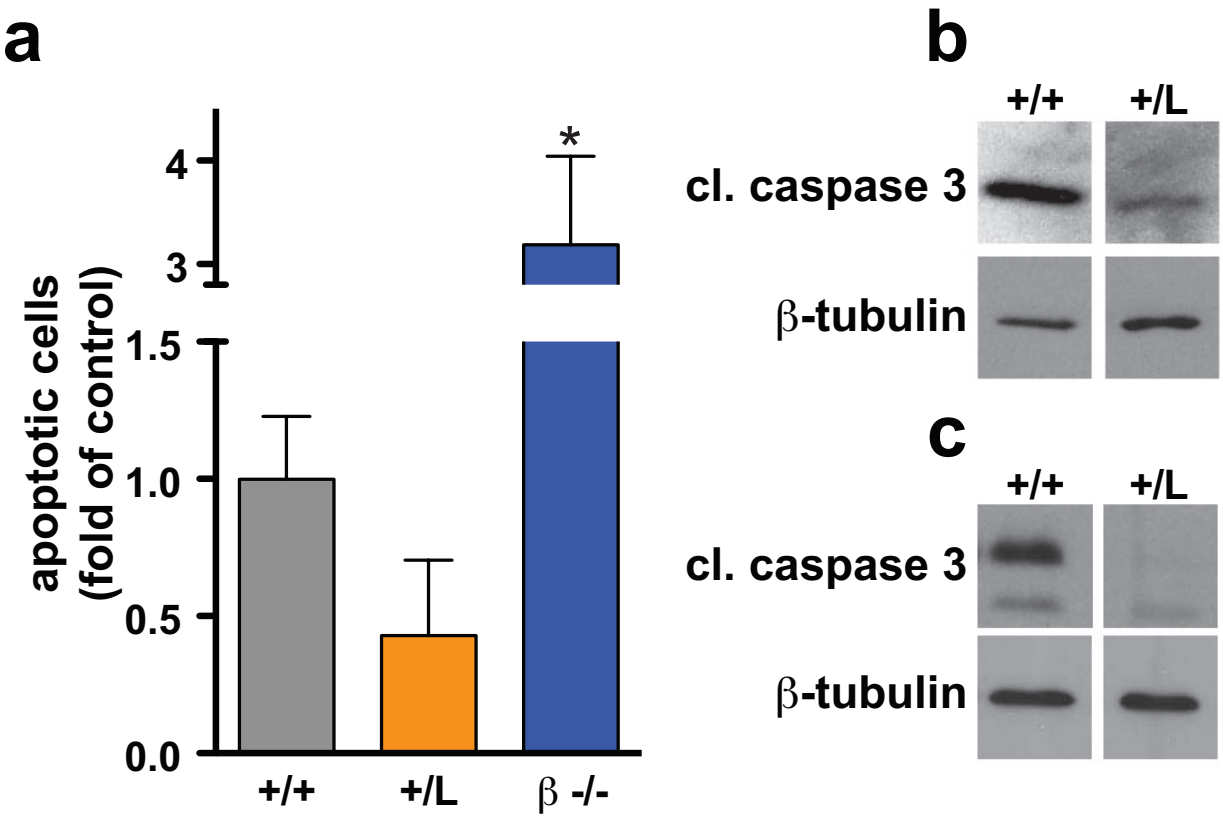
a
apoptotic cells
(fold of control)
4
3
1.5
1.0
0.5
0.0
*
+/+
+/L
β -/-
b
+/+
+/L
cl. caspase 3
β-tubulin
c
+/+
+/L
cl. caspase 3
β-tubulin

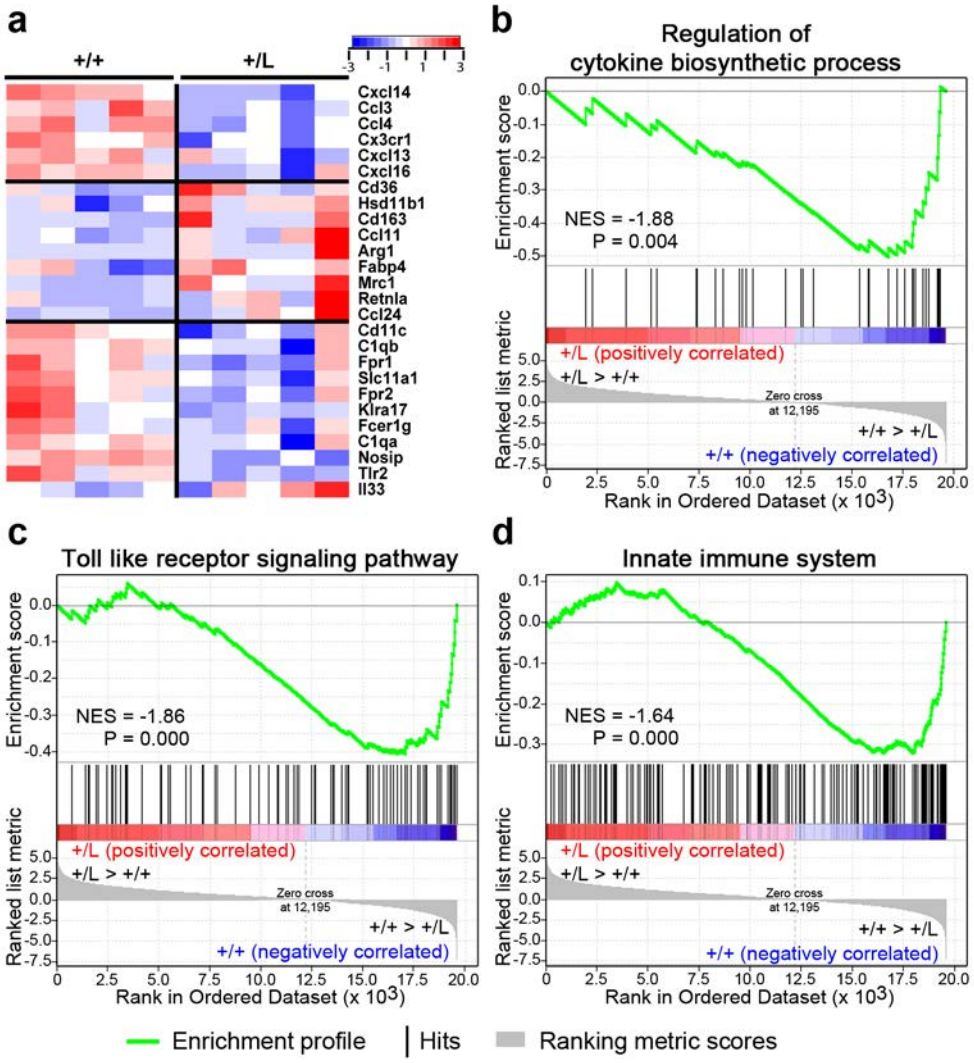
a
+/+
+/L
-3
-1
1
3
Cxcl14
Ccl3
Ccl4
Cx3cr1
Cxcl13
Cxcl16
Cd36
Hsd11b1
Cd163
Ccl11
Arg1
Fabp4
Mrc1
Retnla
Ccl24
Cd11c
C1qb
Fpr1
Slc11a1
Fpr2
Klra17
Fcer1g
C1qa
Nosip
Tlr2
Il33
b
Regulation of
cytokine biosynthetic process
Enrichment score
NES = -1.88
P = 0.004
Ranked list metric
+/L (positively correlated)
+/L > +/+
Zero cross
at 12,195
+/+ > +/L
+/+ (negatively correlated)
Rank in Ordered Dataset (x 10^3)
c
Toll like receptor signaling pathway
Enrichment score
NES = -1.86
P = 0.000
Ranked list metric
+/L (positively correlated)
+/L > +/+
Zero cross
at 12,195
+/+ > +/L
+/+ (negatively correlated)
Rank in Ordered Dataset (x 10^3)
d
Innate immune system
Enrichment score
NES = -1.64
P = 0.000
Ranked list metric
+/L (positively correlated)
+/L > +/+
Zero cross
at 12,195
+/+ > +/L
+/+ (negatively correlated)
Rank in Ordered Dataset (x 10^3)
Enrichment profile
Hits
Ranking metric scores

Journal of Molecular Medicine

SUPPLEMENTARY MATERIAL

Deregulation of the endogenous C/EBPβ LIP isoform predisposes to tumorigenesis

Valérie Bégay, Jeske J. Smink, Christoph Loddenkemper, Karin Zimmermann, Cornelia Rudolph, Marina Scheller, Doris Steinemann, Ulf Leser, Brigitte Schlegelberger, Harald Stein and Achim Leutz.

Corresponding author: Achim Leutz, Univ.-Prof. Dr. rer. nat., Max Delbrueck Center for Molecular Medicine, Dept of Tumorigenesis and Cell Differentiation, Robert-Roessle-Str.10, 13125 BERLIN Germany. Phone: + 49 30 9406 3735, Fax: + 49 30 9406 3298, Email: aleutz@mdc-berlin.de.

SUPPLEMENTARY METHODS

Animals. C57BL/6 Ly5.1 (carrying the CD45.1 marker, also called B6-SJL) congenic mice were originally obtained from Charles River Laboratoires, crossed to 129-Ola (carrying the marker CD45.2) mice to generate 129 X C57BL/6 (CD45.1/CD45.2, called B6-SJL;129-Ola) mice used as donors for bone marrow (BM) cell transplantation. Four to 5 months-old WT and L/L recipient mice (CD45.2) were kept on 129 X C57BL/6 genetic background.

Mouse transplantation experiments. Freshly isolated BM cells were injected (2 X 10^6 cells/mouse) through the tail vein into lethally irradiated (9.5-10 Gy total body irradiation, Cs-137 source) WT or L/L recipient mice. Six weeks after transplantation, repopulation/engraftment was determined and then every 4 weeks by collection of peripheral blood, erythrocyte lysis, and staining of CD45.1 and CD45.2.

Immunohistochemistry (IHC) and analysis. Detection of C/EBPβ (C19, Santa Cruz), Ki67 (Tec-3; Dako), CD3 (n° 1580; Dako); Pax5 (24, Transduction Laboratories), or F4/80 (eBioscience) was performed in paraffin embedded tissue as

described in the manuscript. Binding of the antibodies was detected by Envision peroxidase kit (K4010, Dako) using diaminobenzidine as chromogenic substrate or by the streptavidin alkaline phosphatase kit (K5005, Dako). Note that the rabbit C/EBPβ antibody (C19, Santa cruz) recognizes the C-terminal part of C/EBPβ therefore all isoforms.

Cell preparation, FACS analysis and CD19+ B cells sorting. Bone marrow (BM) cell suspensions were prepared by flushing femurs and tibias with PBS. Single-cell suspensions were prepared from 2/3 of the spleen dissected from 12 or 13-month-old mice, and histopathology analysis was performed on the third part of the spleen as described in the manuscript. Spleen cell suspensions were obtained by gentle disruption of the organ through a cell strainer (70µm, BD Falcon) in PBS/2% fetal calf serum. Peripheral blood (PB) samples were obtained from the tail vein and collected into EDTA coated tubes. The blood cell counts were measured with an automated veterinary hematological counter Scil Vet abc (SCIL GmbH, Viernheim, Germany), with software optimized for mouse blood parameters. Red blood cells (RBC) were lysed on ice with hypotonic erythrocyte lysis buffer (BD Pharmlyse buffer). Non specific binding was reduced by preincubation with unconjugated antibody to FcγRII/III (2.4G2, BD Pharmingen^{TM}) prior to labeling in FACS buffer (PBS, 0,5% BSA, 2mM EDTA). Dead cells were excluded by propidium iodide or 7-AAD staining. Cell staining and sorting were performed using fluorescein isothiocyanate (FITC), phycoerythrin (PE), allophycocyanin (APC) labeled monoclonal antibodies directed against CD45.1 (A20), CD45.2 (104), B220 (6B2), CD19 (1D3), CD3 (KT31.1) and Mac1/CD11b (M1/70) (BD Biosciences, eBioscience and Biolegend). Cells were sorted on FACS ARIA and data were acquired on a LSRII flow cytometers (Becton Dickinson), and were further analyzed with FlowJo software (TreeStar).

Spectral karyotyping. Metaphase chromosomes were prepared by treating cells with colcemid at a final concentration of 0.035 µg/ml overnight, incubated in 0.075 M KCL for 20 min at 37°C and fixed in a freshly prepared mixture of methanol:acetic acid (3:1) at room temperature. Cell suspension was dropped onto glass slides in a climate chamber (Polymer, Kassel, Germany) at 22°C and 48% humidity. Spectral karyotyping (SKY) was performed as described previously (1) and according to the manufacturer's instructions (ASI: Applied Spectra Imaging, Ltd., Migdal HaEmek, Israel). Spectral images were acquired using an epifluorescence microscope equipped with an interferometer (SpectraCube^{TM} ASI), a custom-designed optical filter and the SkyView^{TM} software (ASI).

SUPPLEMENTARY REFERENCE

1. Rudolph C and Schlegelberger B (2009) Spectral karyotyping and fluorescence in situ hybridization of murine cells. *Methods in molecular biology* (Clifton, N.J) **506**: 453-466.

Bégay et al. Figure S1

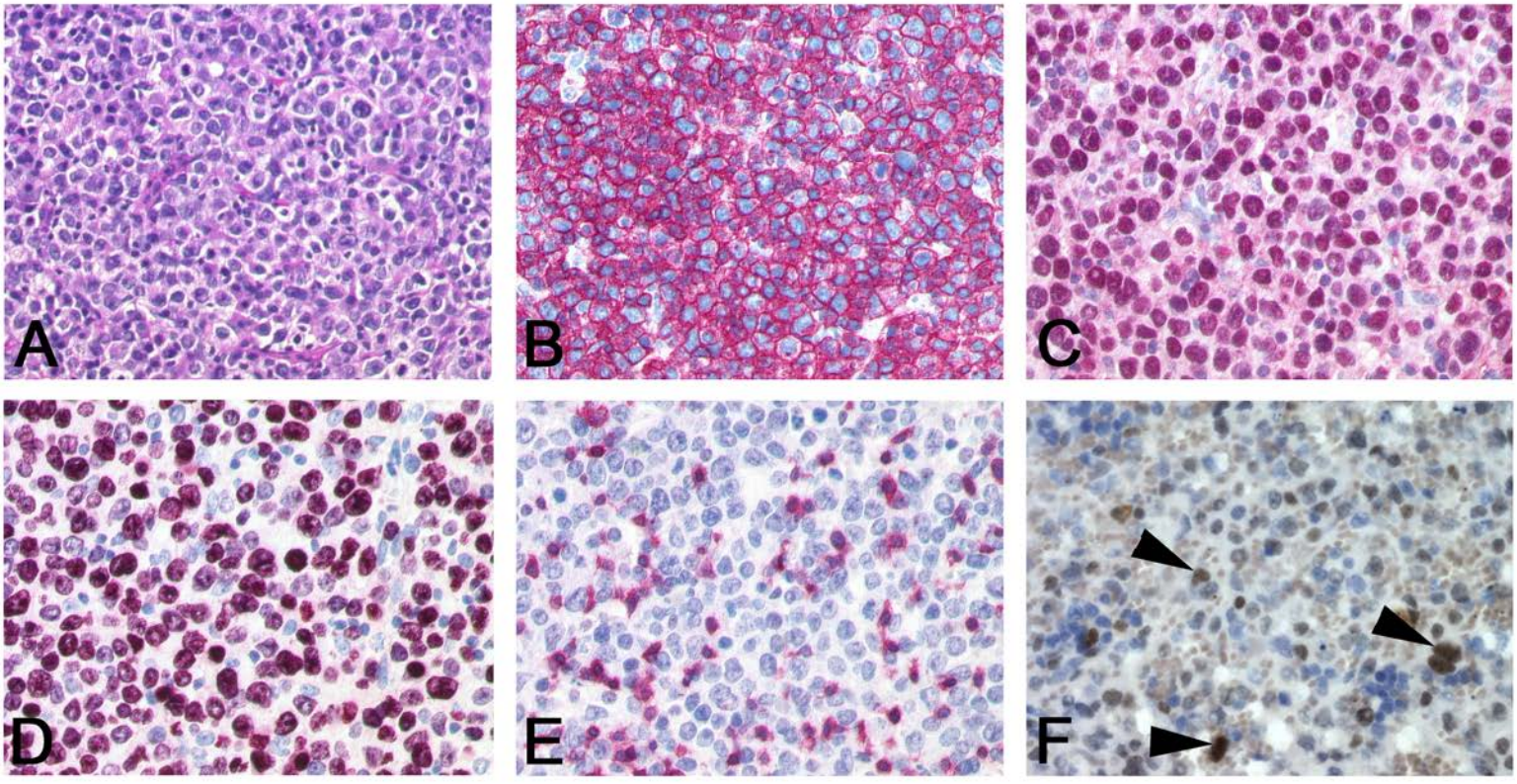

Fig S1. Characterization of B-NHL developed in LIP ki mice. Histological analyses of B-NHL with hematoxylin-eosin staining (**A**). (**B-F**) Immunohistochemical characterization of a B cell lymphoma (diffuse large B cell lymphoma) with strong expression of the B cell markers B220 (**B**) and Pax5 (**C**), showing a high proliferation rate visualized by Ki-67 immunostaining (**D**) and with some admixed reactive T-cells (CD3 positive cells) (**E**) and nuclear expression of C/EBPβ (arrowheads, **F**).
Magnification x 400 for all micrographs.

Bégay et al. Figure S2

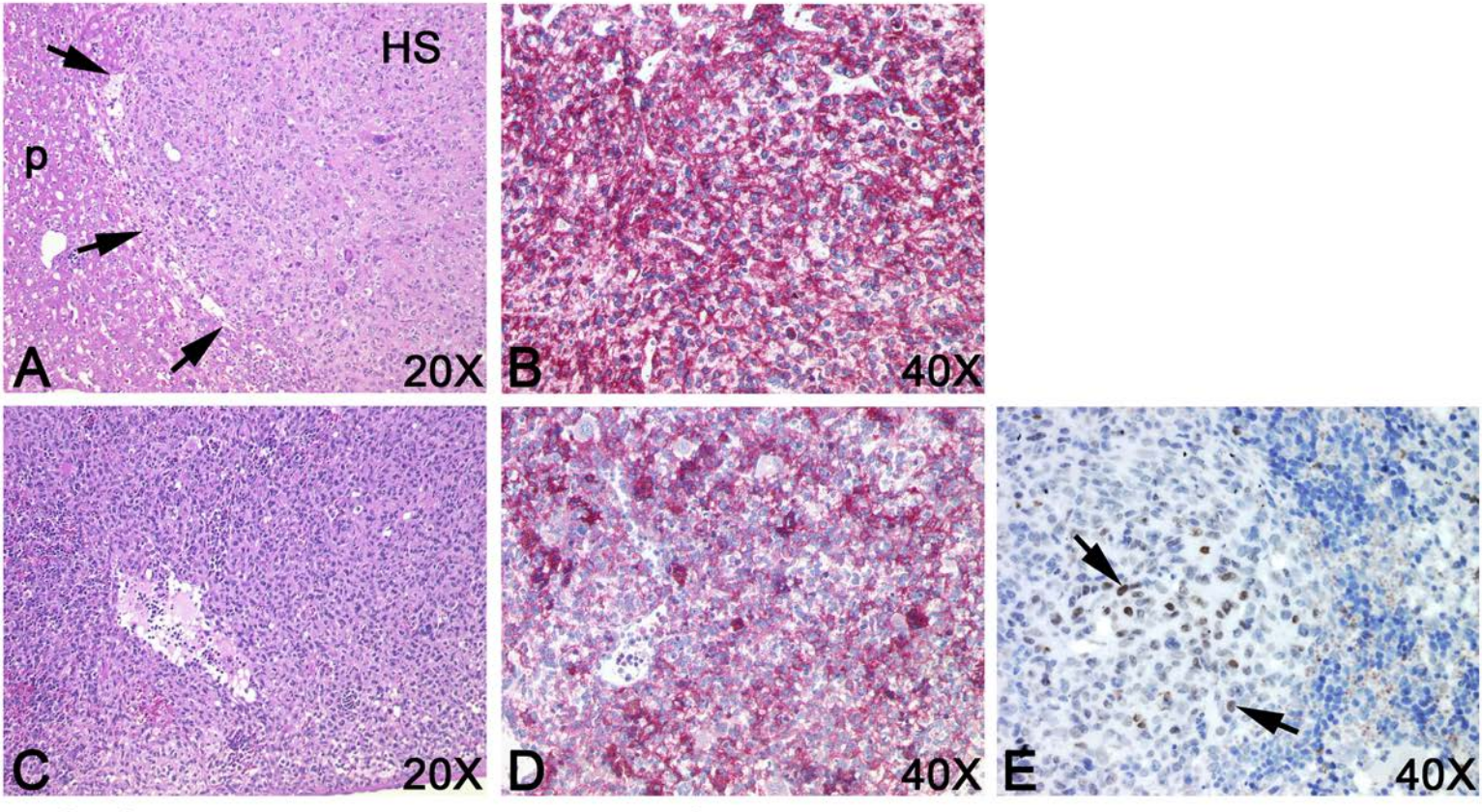

Fig S2. Characterization of histiocytic sarcoma (HS) developed in LIP ki mice.
Hematoxylin and eosin staining of histiocytic sarcoma from liver (**A**) and spleen (**C**) of LIP ki mice. Positive immunostaining for the macrophage marker F4/80 characterized the presence of HS in the liver (**B**) and in the spleen (**D**). Nuclear expression of C/EBPβ (arrows, **E**).
p: liver parenchyma; arrows: HS in **A**.

Bégay et al., Figure S3

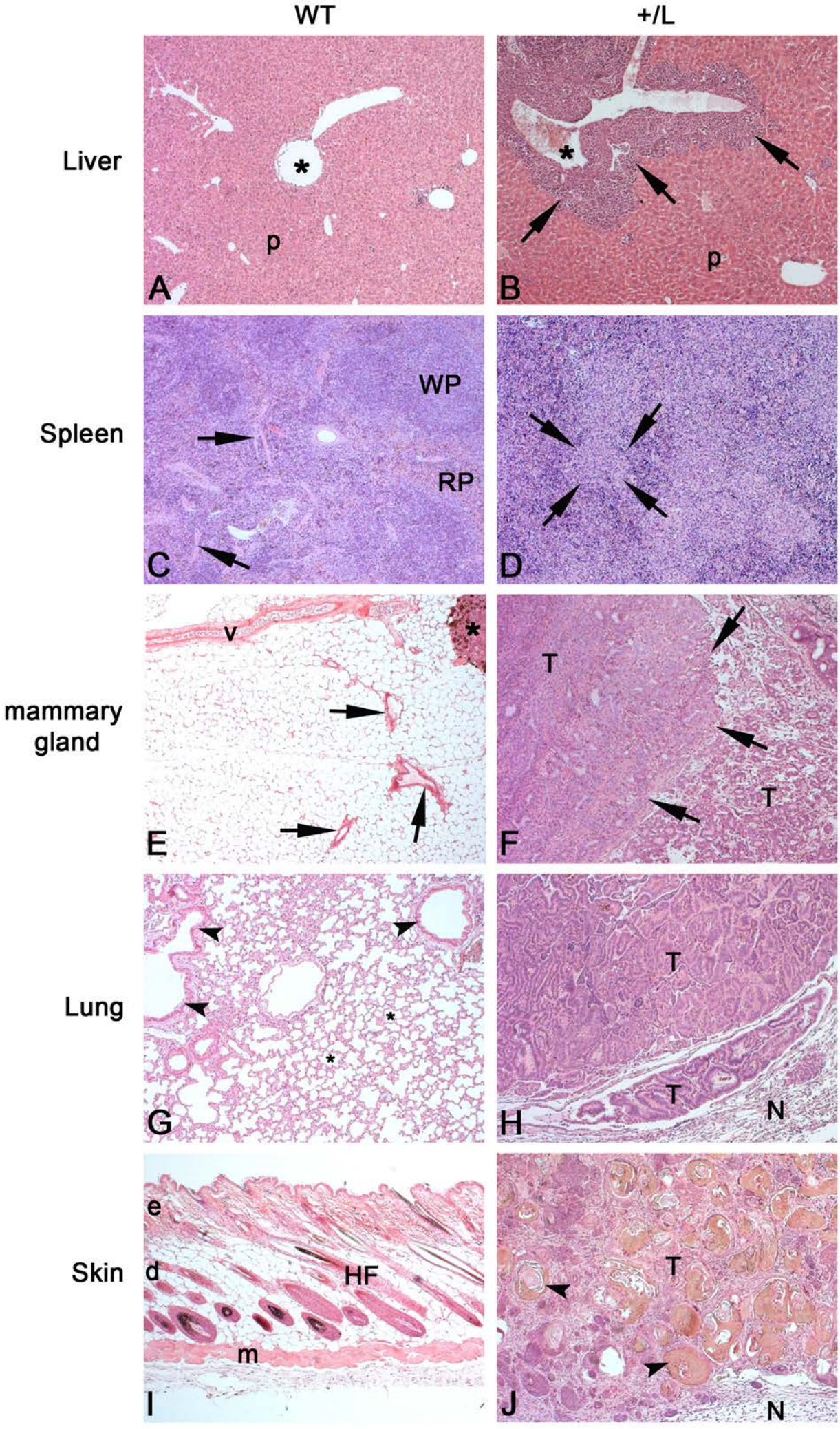

Fig S3. Histological analysis (H&E staining) of hematopoietic (**B**, **D**) and epithelial (**F**, **H** and **J**) tumors found in +/L mice in comparison with control tissues from age-matched WT mice (**A**, **C**, **E**, **G** and **I**) at low magnification. (**A**) Liver with normal parenchyma (p), vein (asterisk). (**B**) Liver with massive infiltration of B cells (arrows), vein (asterisk) (**C**) Normal splenic architecture with white pulp (WP), red pulp (RP) and trabeculae (arrows). (**D**) Histiocytic sarcoma with nodular infiltrates (arrows) developed in the spleen. (**E**) Mammary gland fad pad with normal epithelium duct (arrows), lymph node (asterisk) and vessel (v). (**F**) Mammary carcinoma developed in mammary fat pad (arrows). (**G**) Normal lung parenchyma with bronchiole (arrowheads) and alveoli (asterisks). (**H**) Lung adenocarcinoma with papillary growth. (**I**) Normal skin architecture with epidermis (e), dermis (d), hair follicle (HF) and muscle (m). (**J**) Skin carcinoma with squamous differentiation and keratinization (arrowheads). T: tumor tissue; N: normal tissue. Magnification x5 for all micrographs.

Bégay et al., Figure S4

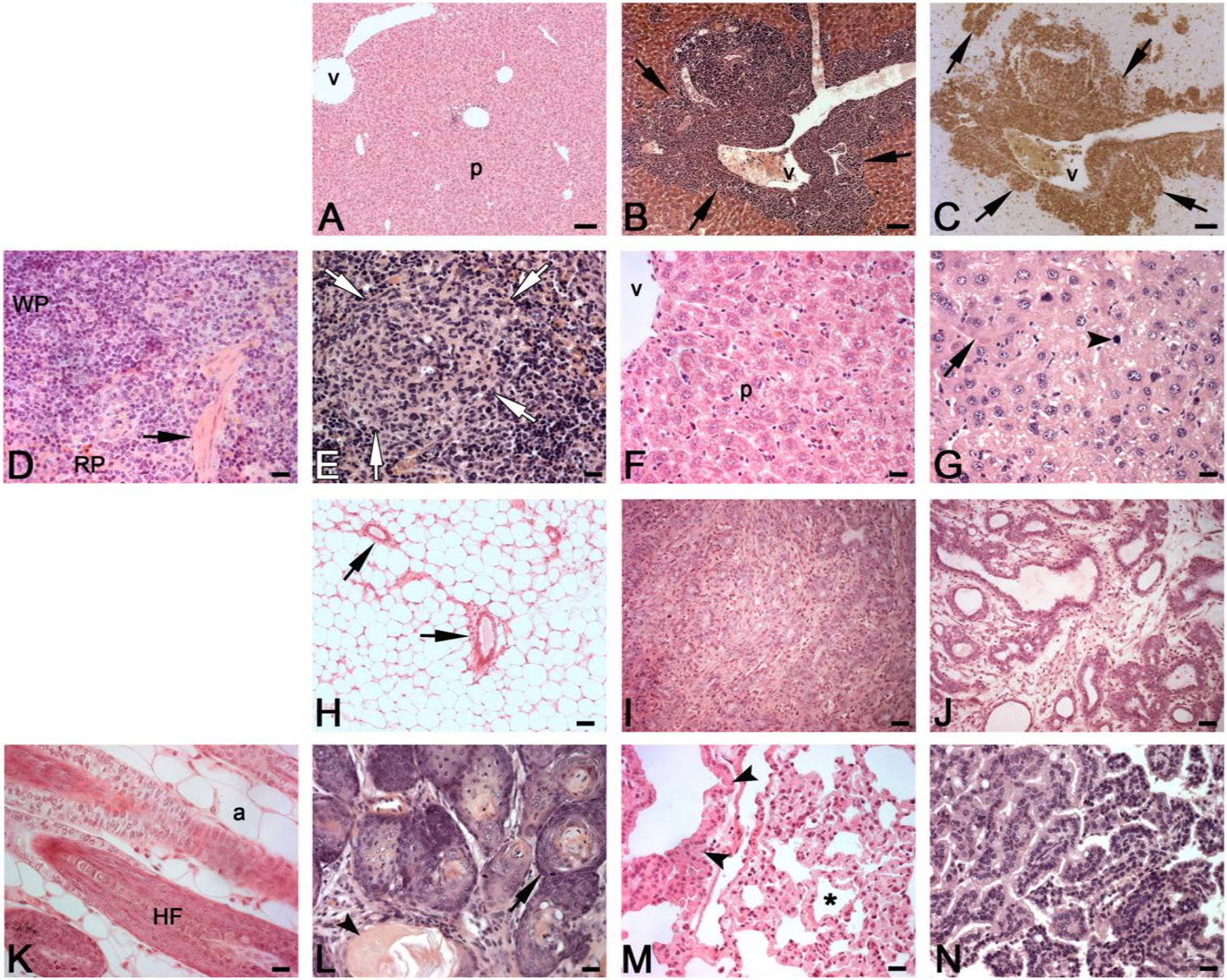

Fig S4. Histological analysis (H&E staining) of hematopoietic (**B**, **C, E**) and epithelial (**G**, **I**, **J, L** and **N**) tumors found in +/L mice in comparison with counterpart tissues from aged-matched WT mice (**A**, **D**, **F**, **H**, **K** and **M**) at higher magnification. (**A**) Liver with normal parenchyma (p). (**B**, **C**) B-NHL with massive infiltration of B cells in the liver (arrows in B) characterized by B220 immunopositive staining (arrows in C). (**D**) Normal splenic architecture with white pulp (WP), red pulp (RP) and trabeculae (arrow). (**E**) Histiocytic sarcoma with nodular infiltrates (arrows) developed in the spleen. (**F**) Liver with normal parenchyma (p). (**G**) Liver with a hepatocellular carcinoma (HCC) showing a trabecular growth pattern (arrow) (arrowhead: mitotic figure). (**H**) Mammary gland fad pad with normal epithelium duct (arrows). (**I**) A ductal and (**J**) a tubular mammary carcinoma developed in mammary fat pad of a +/L female. (**K**) Normal skin architecture with hair follicle (HF) and adipocytes (a). (**J**) Skin carcinoma with squamous differentiation and keratinization (arrowhead) and horn pearl formation (arrow). (**M**) Normal lung parenchyma with bronchiole (arrowheads) and alveoli (asterisk). (**N**) Lung adenocarcinoma with papillary growth. p: parenchyma; v: vein. A, B, C: scale bar = 25 μm; D-G, K-N: scale bar = 20 μm; H-J: scale bar = 10 μm.

Bégay et al., Figure S5

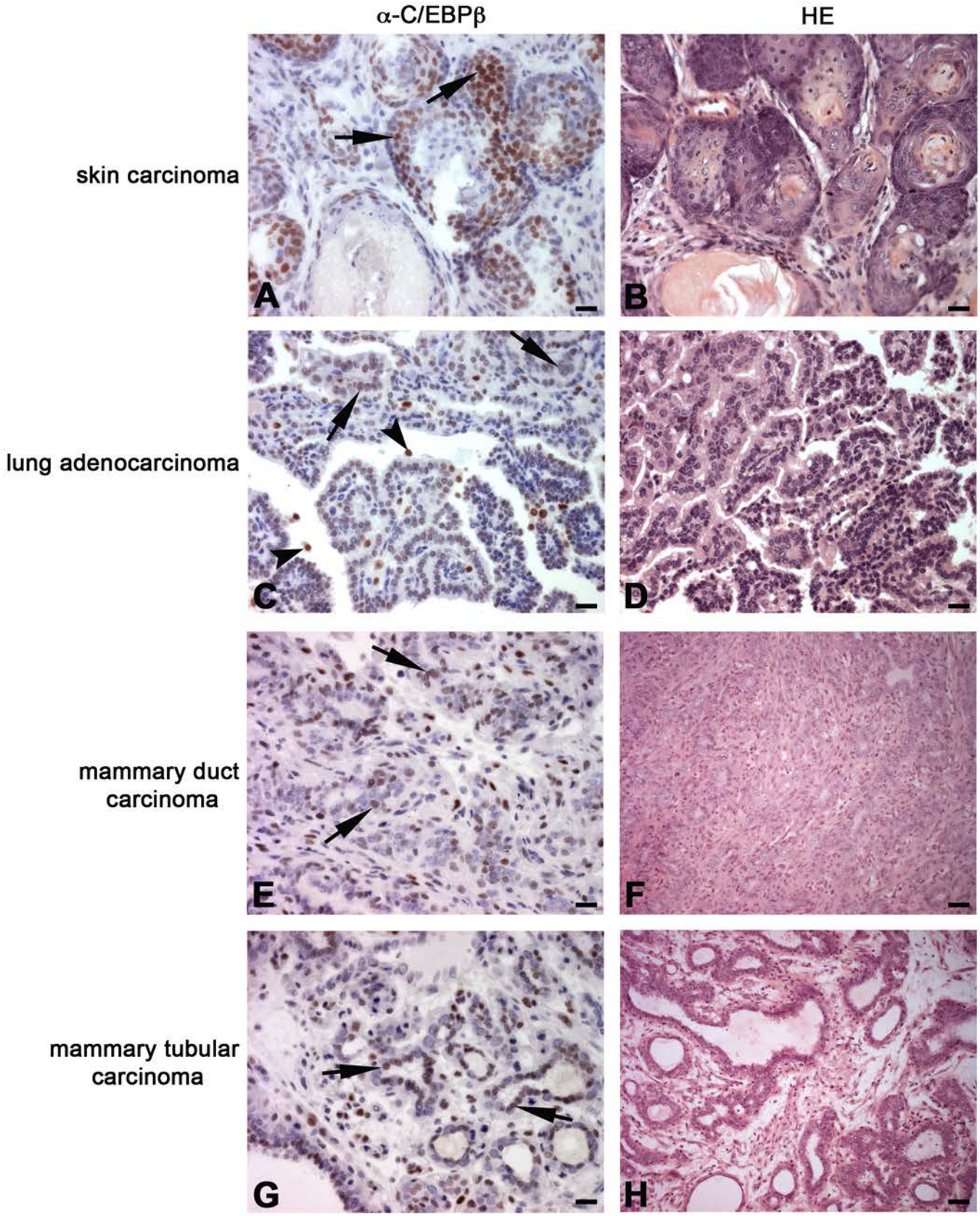

Fig S5. C/EBPβ expression in tumors found in LIP ki mice. Immunostaining of C/EBPβ and H&E staining in tumors found in +/L mice. (**A-B**) skin carcinoma, (**C, D**) lung adenocarcinoma, (**E, F**) ductal and (**G, H**) tubular mammary carcinoma. C/EBPβ immunostaining in blood cells (arrowhead) and tumor cells (arrows). A-E, G: scale bar = 20 μm; F, H: scale bar = 10 μm.

Bégay et al., Figure S6

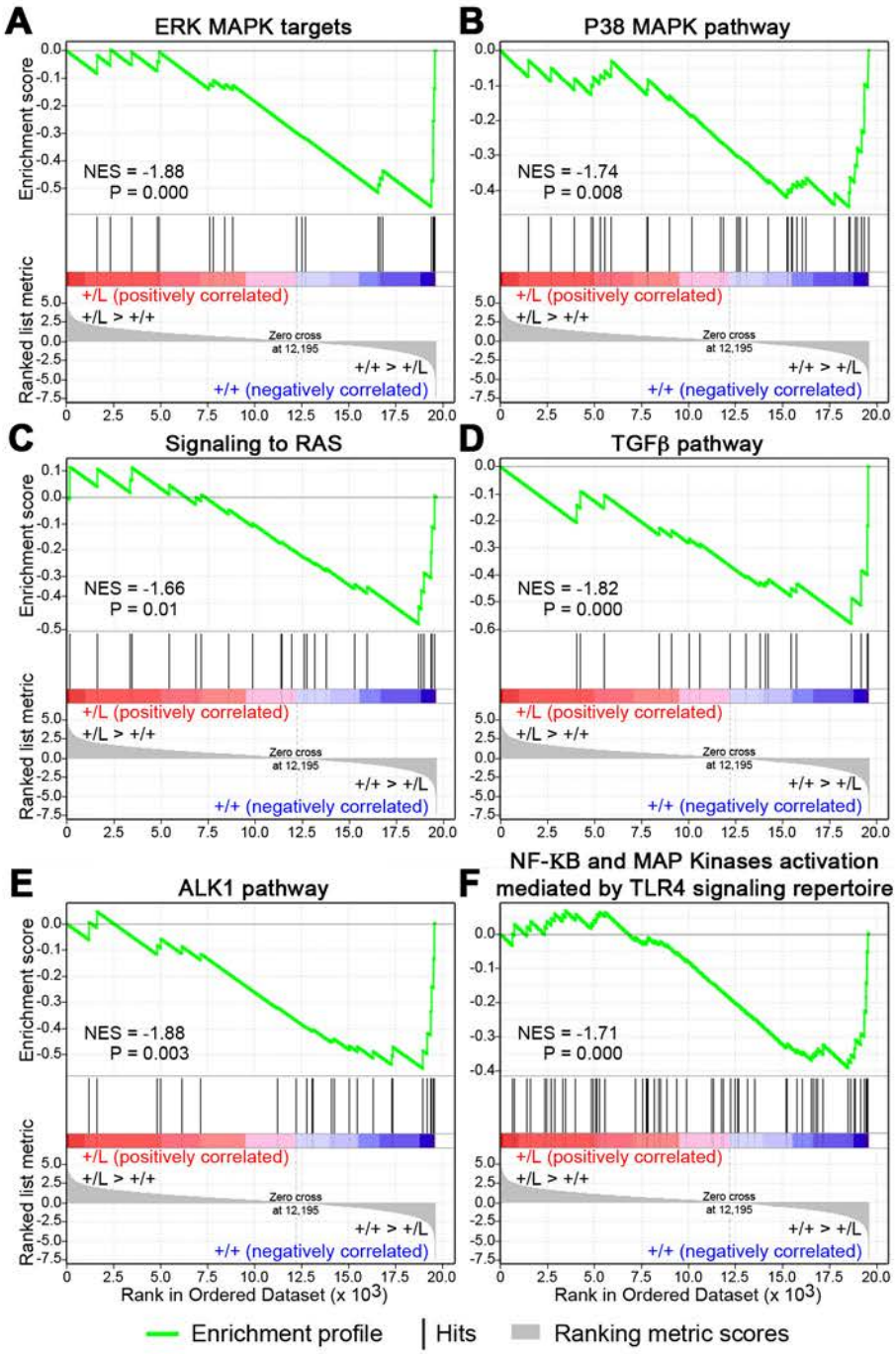

Fig S6. GSEA comparison of signaling pathways between +/L and WT B-NHL. (**A-F**) GSEA based on the comparison of +/L and WT B-NHL for enrichment or depletion of ERK MAPK targets (**A**), P38MAPK pathway (**B**), reactome signaling to RAS (**C**), TGFβ pathway (**D**), ALK1 pathway (**E**) and the reactome NF-kB and MAP Kinases activation mediated by TLR4 signaling repertoire (**F**) associated genes. The normalized enrichment scores (NES) and P values are indicated in each plot. Note that the negative value of the NES indicates a depletion of genes in the depicted gene sets in +/L B-NHL compared to WT B-NHL.

Bégay et al. Figure S7

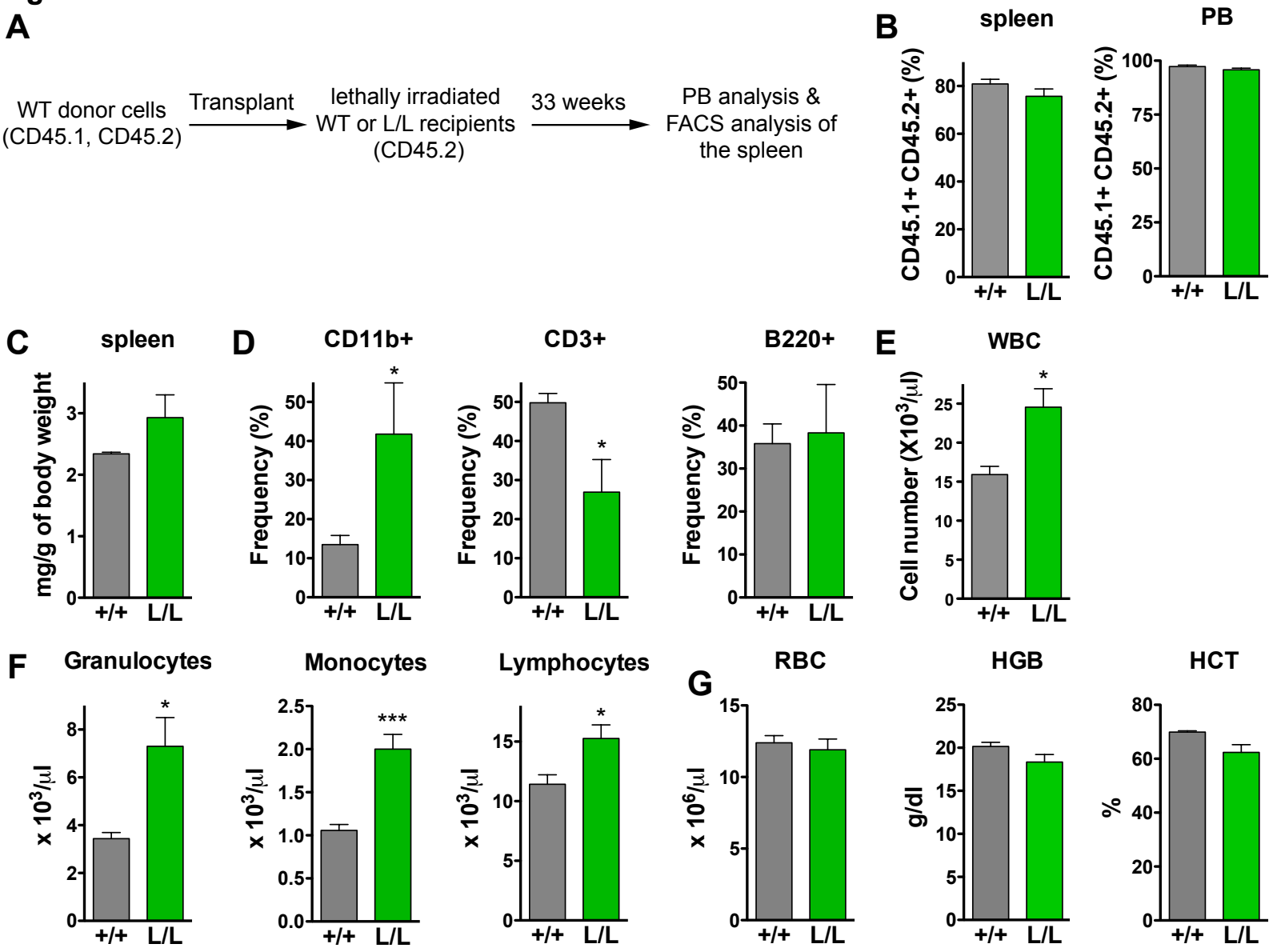

Fig S7. C/EBPβ LIP niche alters hematopoietic cell distribution in the peripheral blood and spleen. (**A**) Schematic representation of the transplantation strategy. Total bone marrow cells (2 X 106) from B6-SJL;129-Ola mice (carrying the CD45.1 and CD45.2 markers) were transplanted into lethally irradiated WT or L/L recipient mice (carrying CD45.2 marker). Recipients were sacrificed 33 weeks after transplantation and the hematopoietic cells of the peripheral blood (PB) and spleen were analyzed by FACS. (**B**) Engraftment of the donor cells (CD45.1+/CD45.2+ cells) in the spleen and peripheral blood (PB). (**C**) Ratio of spleen weight versus body weight. (**D**) Distribution of myeloid cells (CD11b+ marker), T cells (CD3+ marker) and B cells (B220+ marker) in the spleen. (**E**) White blood cell (WBC) count measured in the peripheral blood. (**F**) Distribution of granulocytes, monocytes and lymphocytes measured in the peripheral blood. (**G**) Red blood cell (RBC) count, hematocrit (HCT) and hemoglobin (HGB) levels measured in the peripheral blood. All graphs represent the +/+ (grey bar) and L/L mice (green bar). n = 5 per genotype. Error bars show SEM. *P<0.05. ***P< 0.001.

Table S1. SKY analysis of B-NHL isolated from LIP ki mice.

Genotype	Tissue[a]	Karyotypes[b]
+/+	spleen	40, XX [9]
+/+	spleen	41-43, XX, **+14**, **+15**, **+17** [cp5]/
		40, XX [10]
+/+	spleen	41, XX, **+15** [4]/
		41, XX, **+17** [2]/
		42, XX, **+15**, **+17** [1]/
		40, XX [8]
+/L	LN	40, XX [10]
+/L	LN	40, XX [8]
+/L	spleen	40, XX [10]
L/L	LN	41, XX, **+X** [3]/
		41, XX, **+X**, **?Del(19)** [cp6]/
		40, XX [5]
L/L	LN	80<**4n**>, XXXX [3]/
		40, XX [11]
L/L	spleen	40, XX [6]/
		80<**4n**>, XXXX [8]
L/L	spleen	40, XX [9]

No chromosomal alterations were observed in 3 analyzed +/L lymphomas. Tetraploid chromosomal complements were seen in L/L lymphomas. Note that 2 out of 3 analyzed lymphomas found in WT carried a trisomy 15 and 17 as clonal chromosomal alterations. B-NHL: B non-Hodgkin's lymphoma. [a] LN: lymph node; [b] Del: deletion, [n]: number of metaphases showing the alteration, [cp]: composite karyotype. Clonal chromosomal alterations are marked in bold.

Table S2. List of deregulated genes in B-NHL of +/L mice.

The Symbol and the annotation of the genes are shown. The fold of change (log2(fc)) and the P value are indicated for each gene.

Symbol	log2(fc)	P value	GeneName
Cfd	3,47	1,72E-02	complement factor D (adipsin)
S100a9	2,89	9,94E-03	S100 calcium binding protein A9 (calgranulin B)
Ccl24	2,78	9,40E-03	chemokine (C-C motif) ligand 24
Htatip2	2,41	1,50E-04	HIV-1 tat interactive protein 2, homolog (human)
Lum	2,32	1,48E-02	lumican
Igfbp5	2,15	8,20E-04	insulin-like growth factor binding protein 5
Cidec	2,13	1,81E-02	cell death-inducing DFFA-like effector c
Postn	2,09	1,56E-02	periostin, osteoblast specific factor
Glycam1	2,09	1,33E-02	glycosylation dependent cell adhesion molecule 1
Retnla	1,99	1,93E-02	resistin like alpha
Mrc1	1,84	8,44E-03	mannose receptor, C type 1
Aldh1a2	1,67	9,40E-04	aldehyde dehydrogenase family 1, subfamily A2
Fabp4	1,62	9,74E-03	fatty acid binding protein 4, adipocyte
Rab15	1,62	1,16E-02	RAB15, member RAS oncogene family
Adipoq	1,58	4,06E-02	adiponectin, C1Q and collagen domain containing
Arg1	1,57	2,35E-02	arginase, liver
Cpe	1,56	3,84E-03	carboxypeptidase E
Plin4	1,52	7,32E-03	perilipin 4
Cbr2	1,48	1,76E-02	carbonyl reductase 2
Fabp7	1,47	1,34E-02	fatty acid binding protein 7, brain
Saa3	1,45	2,11E-02	serum amyloid A 3
Fam103a1	1,45	2,00E-05	family with sequence similarity 103, member A1
Malat1	1,39	3,95E-03	metastasis associated lung adenocarcinoma transcript 1 (non-coding RNA)
Cma1	1,33	5,75E-03	chymase 1, mast cell
Fus	1,33	2,60E-04	fusion, derived from t(12;16) malignant liposarcoma (human)
Clec2d	1,30	1,98E-02	C-type lectin domain family 2, member d
Cfh	1,30	2,21E-02	complement component factor h
Ccl11	1,29	8,54E-03	chemokine (C-C motif) ligand 11
Cd163	1,27	6,44E-03	CD163 antigen
BC018465	1,25	1,59E-03	cDNA sequence BC018465
Aldh1a3	1,25	1,30E-02	aldehyde dehydrogenase family 1, subfamily A3
Gadd45g	1,25	1,79E-03	growth arrest and DNA-damage-inducible 45 gamma
Madcam1	1,25	1,13E-02	mucosal vascular addressin cell adhesion molecule 1
Il33	1,24	1,55E-02	interleukin 33
Gas6	1,23	3,08E-03	growth arrest specific 6
Plin1	1,23	3,71E-02	perilipin 1
Dpt	1,22	3,16E-03	dermatopontin
Fam174b	1,21	1,10E-02	family with sequence similarity 174, member B
Hdc	1,19	6,75E-03	histidine decarboxylase
Metrn	1,17	3,00E-05	meteorin, glial cell differentiation regulator
Folr2	1,16	3,46E-02	folate receptor 2 (fetal)
Surf6	1,15	3,00E-05	surfeit gene 6
Dnajc7	1,14	1,96E-03	DnaJ (Hsp40) homolog, subfamily C, member 7
Snord123	1,13	3,18E-03	small nucleolar RNA, C/D box 123
Hbb-bh1	1,13	3,96E-02	hemoglobin Z, beta-like embryonic chain
Figf	1,11	6,84E-03	c-fos induced growth factor
Echdc2	1,10	4,59E-02	enoyl Coenzyme A hydratase domain containing 2
Agt	1,09	3,01E-02	angiotensinogen (serpin peptidase inhibitor, clade A, member 8)
Scgb3a1	1,09	1,71E-02	secretoglobin, family 3A, member 1
Mcpt4	1,09	1,35E-02	mast cell protease 4
Ppp3ca	1,08	3,00E-05	protein phosphatase 3, catalytic subunit, alpha isoform
Themis	1,08	1,96E-02	thymocyte selection associated
Hsd11b1	1,06	4,96E-02	hydroxysteroid 11-beta dehydrogenase 1
Nkx2-3	1,05	1,06E-02	NK2 transcription factor related, locus 3 (Drosophila)
Cyfip1	1,04	8,31E-03	cytoplasmic FMR1 interacting protein 1
Prmt1	1,04	1,82E-03	protein arginine N-methyltransferase 1
Atp1a2	1,04	5,02E-03	ATPase, Na+/K+ transporting, alpha 2 polypeptide
Tmed9	1,03	2,30E-04	transmembrane emp24 protein transport domain containing 9
1500012F01Rik	1,03	2,20E-04	RIKEN cDNA 1500012F01 gene

Symbol	log2(fc)	P value	GeneName
C6	1,03	7,51E-03	complement component 6
Ly9	1,01	1,00E-04	lymphocyte antigen 9
Cd36	1,01	3,15E-02	CD36 antigen
Vapb	1,01	7,10E-03	vesicle-associated membrane protein, associated protein B and C
Cited4	1,01	3,70E-02	Cbp/p300-interacting transactivator, with Glu/Asp-rich carboxy-terminal domain, 4
Ces3	1,01	4,37E-03	carboxylesterase 3
Cox6c	1,01	0,00E+00	cytochrome c oxidase, subunit VIc
Tlr2	-1,00	1,03E-03	toll-like receptor 2
Rnd3	-1,00	2,06E-02	Rho family GTPase 3
9830001H06Rik	-1,00	9,30E-04	RIKEN cDNA 9830001H06 gene
1700112E06Rik	-1,00	3,26E-03	RIKEN cDNA 1700112E06 gene
D6Mm5e	-1,01	2,04E-02	DNA segment, Chr 6, Miriam Meisler 5, expressed
Lpcat2	-1,02	1,40E-03	lysophosphatidylcholine acyltransferase 2
Pigz	-1,02	1,37E-03	phosphatidylinositol glycan anchor biosynthesis, class Z
Tm6sf2	-1,02	4,73E-02	transmembrane 6 superfamily member 2
Hist1h2ak	-1,03	5,90E-04	histone cluster 1, H2ak
Nr1h3	-1,04	4,06E-02	nuclear receptor subfamily 1, group H, member 3
Abhd2	-1,05	1,23E-03	abhydrolase domain containing 2
Zmynd15	-1,06	2,79E-03	zinc finger, MYND-type containing 15
Hist1h1e	-1,06	6,14E-03	histone cluster 1, H1e
Niacr1	-1,08	1,43E-03	niacin receptor 1
Hist1h2ai	-1,08	4,30E-04	histone cluster 1, H2ai
Cxcl16	-1,10	3,26E-03	chemokine (C-X-C motif) ligand 16
Nosip	-1,11	1,66E-03	nitric oxide synthase interacting protein
C1qa	-1,11	3,91E-02	complement component 1, q subcomponent, alpha polypeptide
Fcer1g	-1,12	2,96E-02	Fc receptor, IgE, high affinity I, gamma polypeptide
8430428J23Rik	-1,13	4,71E-02	RIKEN cDNA 8430428J23 gene
Hyi	-1,14	7,62E-03	hydroxypyruvate isomerase homolog (E. coli)
Ltbp2	-1,15	1,14E-02	latent transforming growth factor beta binding protein 2
Kcnj10	-1,15	1,01E-03	potassium inwardly-rectifying channel, subfamily J, member 10
Gdf3	-1,17	1,24E-02	growth differentiation factor 3
Lsm14b	-1,18	8,00E-05	LSM14 homolog B (SCD6, S. cerevisiae)
Batf2	-1,19	1,20E-02	basic leucine zipper transcription factor, ATF-like 2
Lst1	-1,19	6,64E-03	leukocyte specific transcript 1
Smpdl3b	-1,19	1,41E-03	sphingomyelin phosphodiesterase, acid-like 3B
Fam20c	-1,20	4,19E-02	family with sequence similarity 20, member C
Klra17	-1,20	8,30E-04	killer cell lectin-like receptor, subfamily A, member 17
Cap1	-1,21	1,67E-03	CAP, adenylate cyclase-associated protein 1 (yeast)
Rdh12	-1,23	4,92E-02	retinol dehydrogenase 12
Il28ra	-1,23	2,64E-02	interleukin 28 receptor alpha
H28	-1,26	1,54E-02	histocompatibility 28
Cxcl13	-1,27	4,92E-02	chemokine (C-X-C motif) ligand 13
C1qb	-1,27	1,47E-02	complement component 1, q subcomponent, beta polypeptide
1810033B17Rik	-1,28	1,51E-02	RIKEN cDNA 1810033B17 gene
Clec4a3	-1,29	3,01E-02	C-type lectin domain family 4, member a3
Cx3cr1	-1,37	1,80E-03	chemokine (C-X3-C) receptor 1
Prim2	-1,37	1,06E-02	DNA primase, p58 subunit
Fpr2	-1,38	3,73E-02	formyl peptide receptor 2
Slc11a1	-1,40	3,65E-03	solute carrier family 11 (proton-coupled divalent metal ion transporters), member 1
Fpr1	-1,42	8,82E-03	formyl peptide receptor 1
Itgax	-1,42	1,53E-02	integrin alpha X
Ccl4	-1,45	7,46E-03	chemokine (C-C motif) ligand 4
Actg2	-1,46	6,00E-05	actin, gamma 2, smooth muscle, enteric
Asb2	-1,48	5,24E-03	ankyrin repeat and SOCS box-containing 2
Ifi202b	-1,59	1,38E-02	interferon activated gene 202B
Kif1a	-1,60	5,00E-05	kinesin family member 1A
Ccl3	-1,61	3,36E-03	chemokine (C-C motif) ligand 3
Rmrp	-1,65	4,00E-05	RNA component of mitochondrial RNAase P
Cxcl14	-1,84	7,60E-04	chemokine (C-X-C motif) ligand 14
Serpina1d	-1,88	1,55E-03	serine (or cysteine) peptidase inhibitor, clade A, member 1D
Sostdc1	-1,89	4,94E-03	sclerostin domain containing 1
Serpina1c	-2,00	5,70E-04	serine (or cysteine) peptidase inhibitor, clade A, member 1C
Serpina1b	-2,19	1,52E-03	serine (or cysteine) preptidase inhibitor, clade A, member 1B
1810009J06Rik	-2,35	5,10E-04	RIKEN cDNA 1810009J06 gene

Table S3. GSEA of deregulated genes found in B-NHL of +/L mice.
The following gene sets from MSigDB data base (http://www.broadinstitute.org/gsea) were used: for human C2: curated gene sets (canonical pathways, Biocarta, KEGG and Reactome); for mouse: C2. The data are shown as positive and negative scoring gene sets listed in order of decreasing statistical significance (P value). The normalized enrichment score (NES), the normalized P value (NOM-P val) and false discovery rate (FDR) are shown.

human C2 negative report

GENE SET NAME	SIZE	NES	NOM p-val	FDR q-val
KEGG_THYROID_CANCER	25	-2,222	0,000	0,021
KEGG_LEISHMANIA_INFECTION	47	-2,165	0,000	0,030
PID_IL27PATHWAY	25	-2,154	0,000	0,023
KEGG_NATURAL_KILLER_CELL_MEDIATED_CYTOTOXICITY	90	-2,125	0,000	0,022
REACTOME_PLATELET_SENSITIZATION_BY_LDL	16	-2,045	0,000	0,043
SA_MMP_CYTOKINE_CONNECTION	15	-2,040	0,000	0,038
BIOCARTA_IL12_PATHWAY	21	-1,977	0,003	0,064
REACTOME_NUCLEAR_EVENTS_KINASE_AND_TRANSCRIPTION_FACTOR_ACTIVATION	23	-1,911	0,000	0,102
BIOCARTA_NTHI_PATHWAY	23	-1,887	0,000	0,110
BIOCARTA_NO2IL12_PATHWAY	15	-1,885	0,000	0,100
BIOCARTA_IL6_PATHWAY	20	-1,884	0,006	0,093
PID_IL23PATHWAY	35	-1,879	0,000	0,088
REACTOME_ERK_MAPK_TARGETS	20	-1,878	0,000	0,082
PID_ALK1PATHWAY	24	-1,877	0,003	0,077
PID_RXR_VDR_PATHWAY	24	-1,875	0,000	0,074
KEGG_TOLL_LIKE_RECEPTOR_SIGNALING_PATHWAY	87	-1,857	0,000	0,080
REACTOME_GLYCOLYSIS	23	-1,854	0,000	0,077
BIOCARTA_NKT_PATHWAY	29	-1,849	0,004	0,075
BIOCARTA_TGFB_PATHWAY	18	-1,819	0,000	0,091
BIOCARTA_DC_PATHWAY	22	-1,804	0,003	0,099
BIOCARTA_FMLP_PATHWAY	33	-1,786	0,000	0,108
KEGG_GRAFT_VERSUS_HOST_DISEASE	16	-1,783	0,009	0,106
KEGG_NOTCH_SIGNALING_PATHWAY	39	-1,772	0,000	0,111
REACTOME_ACTIVATED_TLR4_SIGNALLING	77	-1,769	0,000	0,109
BIOCARTA_HCMV_PATHWAY	17	-1,747	0,007	0,124
BIOCARTA_P38MAPK_PATHWAY	37	-1,736	0,008	0,129
REACTOME_TOLL_RECEPTOR_CASCADES	94	-1,715	0,000	0,144
REACTOME_NFKB_AND_MAP_KINASES_ACTIVATION_MEDIATED_BY_TLR4_SIGNALING_REPERTOIRE	60	-1,713	0,000	0,140
SIG_INSULIN_RECEPTOR_PATHWAY_IN_CARDIAC_MYOCYTES	47	-1,710	0,008	0,138
REACTOME_MAPK_TARGETS_NUCLEAR_EVENTS_MEDIATED_BY_MAP_KINASES	29	-1,705	0,007	0,138
KEGG_CHRONIC_MYELOID_LEUKEMIA	69	-1,684	0,000	0,157
REACTOME_RNA_POL_I_PROMOTER_OPENING	23	-1,681	0,007	0,155
PID_FCER1PATHWAY	54	-1,679	0,000	0,153
REACTOME_P75_NTR_RECEPTOR_MEDIATED_SIGNALLING	71	-1,675	0,000	0,153
BIOCARTA_IL2_PATHWAY	20	-1,666	0,019	0,159
ST_T_CELL_SIGNAL_TRANSDUCTION	43	-1,665	0,004	0,156
PID_P38_MK2PATHWAY	21	-1,664	0,003	0,152
REACTOME_SIGNALLING_TO_RAS	24	-1,659	0,010	0,154
REACTOME_MYD88_MAL_CASCADE_INITIATED_ON_PLASMA_MEMBRANE	68	-1,658	0,000	0,151
PID_IL12_STAT4PATHWAY	29	-1,655	0,022	0,150
PID_IL12_2PATHWAY	54	-1,653	0,009	0,150
BIOCARTA_TOB1_PATHWAY	18	-1,648	0,016	0,152
PID_RETINOIC_ACID_PATHWAY	26	-1,646	0,017	0,151

GENE SET NAME	SIZE	NES	NOM p-val	FDR q-val
REACTOME_INNATE_IMMUNE_SYSTEM	166	-1,644	0,000	0,150
REACTOME_PACKAGING_OF_TELOMERE_ENDS	22	-1,641	0,007	0,149
KEGG_DORSO_VENTRAL_AXIS_FORMATION	21	-1,635	0,017	0,152
BIOCARTA_G1_PATHWAY	27	-1,633	0,007	0,151
BIOCARTA_IL10_PATHWAY	17	-1,628	0,028	0,153
ST_B_CELL_ANTIGEN_RECEPTOR	37	-1,624	0,008	0,154
BIOCARTA_TNFR2_PATHWAY	18	-1,613	0,023	0,162
REACTOME_COSTIMULATION_BY_THE_CD28_FAMILY	50	-1,608	0,000	0,163
BIOCARTA_PYK2_PATHWAY	24	-1,604	0,026	0,164
REACTOME_INTERFERON_ALPHA_BETA_SIGNALING	40	-1,604	0,012	0,162
PID_NFKAPPABATYPICALPATHWAY	16	-1,602	0,050	0,161
SA_G1_AND_S_PHASES	15	-1,601	0,031	0,159
KEGG_SYSTEMIC_LUPUS_ERYTHEMATOSUS	59	-1,601	0,000	0,156
BIOCARTA_INTEGRIN_PATHWAY	34	-1,593	0,015	0,163
PID_ANTHRAXPATHWAY	16	-1,589	0,034	0,165
KEGG_RENAL_CELL_CARCINOMA	66	-1,579	0,005	0,173
BIOCARTA_NKCELLS_PATHWAY	18	-1,579	0,044	0,171
REACTOME_THE_ROLE_OF_NEF_IN_HIV1_REPLICATION_AND_DISEASE_PATHOGENESIS	24	-1,571	0,022	0,177
BIOCARTA_BCR_PATHWAY	30	-1,566	0,015	0,180
KEGG_JAK_STAT_SIGNALING_PATHWAY	127	-1,566	0,000	0,178
BIOCARTA_EPO_PATHWAY	17	-1,562	0,042	0,178
PID_PDGFRBPATHWAY	118	-1,561	0,000	0,178
BIOCARTA_CTCF_PATHWAY	22	-1,560	0,038	0,175
PID_IL2_1PATHWAY	51	-1,551	0,012	0,184
SA_B_CELL_RECEPTOR_COMPLEXES	22	-1,546	0,037	0,187
BIOCARTA_INFLAM_PATHWAY	26	-1,546	0,022	0,185
BIOCARTA_SPRY_PATHWAY	16	-1,541	0,043	0,188
KEGG_CYSTEINE_AND_METHIONINE_METABOLISM	28	-1,535	0,027	0,192
BIOCARTA_MAPK_PATHWAY	82	-1,532	0,000	0,193
REACTOME_SIGNALING_BY_RHO_GTPASES	85	-1,531	0,006	0,191
PID_GMCSF_PATHWAY	33	-1,531	0,024	0,189
REACTOME_MUSCLE_CONTRACTION	41	-1,529	0,017	0,189
SIG_PIP3_SIGNALING_IN_CARDIAC_MYOCTES	61	-1,528	0,000	0,187
KEGG_PRION_DISEASES	29	-1,526	0,030	0,188
REACTOME_TRAF6_MEDIATED_INDUCTION_OF_NFKB_AND_MAP_KINASES_UPON_TLR7_8_OR_9_ACTIVATION	63	-1,524	0,010	0,188
BIOCARTA_ERYTH_PATHWAY	15	-1,523	0,029	0,186
BIOCARTA_CXCR4_PATHWAY	20	-1,523	0,017	0,184
BIOCARTA_IL1R_PATHWAY	31	-1,519	0,032	0,184
REACTOME_MAP_KINASE_ACTIVATION_IN_TLR_CASCADE	42	-1,515	0,024	0,186
PID_MAPKTRKPATHWAY	30	-1,515	0,021	0,185
BIOCARTA_IL22BP_PATHWAY	16	-1,514	0,034	0,184
PID_RAC1_REG_PATHWAY	31	-1,511	0,022	0,183
BIOCARTA_NFKB_PATHWAY	22	-1,501	0,046	0,192
BIOCARTA_KERATINOCYTE_PATHWAY	42	-1,494	0,020	0,199
REACTOME_SIGNALLING_TO_ERKS	32	-1,492	0,040	0,198
REACTOME_TRIF_MEDIATED_TLR3_SIGNALING	62	-1,492	0,009	0,197
BIOCARTA_TOLL_PATHWAY	32	-1,491	0,032	0,196
BIOCARTA_NGF_PATHWAY	15	-1,489	0,050	0,196
KEGG_VIRAL_MYOCARDITIS	45	-1,489	0,021	0,194
BIOCARTA_RELA_PATHWAY	16	-1,489	0,048	0,192
REACTOME_IL_2_SIGNALING	37	-1,488	0,012	0,192
KEGG_FC_EPSILON_RI_SIGNALING_PATHWAY	74	-1,487	0,014	0,190
PID_UPA_UPAR_PATHWAY	39	-1,474	0,030	0,205
PID_AR_PATHWAY	42	-1,471	0,032	0,205
KEGG_T_CELL_RECEPTOR_SIGNALING_PATHWAY	101	-1,470	0,000	0,203

GENE SET NAME	SIZE	NES	NOM p-val	FDR q-val
PID_IL8CXCR2_PATHWAY	27	-1,468	0,035	0,205
KEGG_B_CELL_RECEPTOR_SIGNALING_PATHWAY	70	-1,468	0,031	0,203
REACTOME_AMYLOIDS	38	-1,464	0,030	0,206
KEGG_TYROSINE_METABOLISM	35	-1,459	0,025	0,210
REACTOME_SIGNALING_BY_ILS	94	-1,452	0,029	0,216
REACTOME_DEVELOPMENTAL_BIOLOGY	320	-1,448	0,000	0,218
BIOCARTA_ALK_PATHWAY	34	-1,445	0,041	0,216
REACTOME_G_ALPHA1213_SIGNALLING_EVENTS	69	-1,444	0,010	0,216
PID_TCR_PATHWAY	58	-1,440	0,020	0,220
PID_P38ALPHABETADOWNSTREAMPATHWAY	35	-1,440	0,015	0,218
KEGG_GLYCOSAMINOGLYCAN_DEGRADATION	20	-1,439	0,047	0,217
PID_FOXM1PATHWAY	37	-1,422	0,031	0,232
REACTOME_SEMAPHORIN_INTERACTIONS	58	-1,411	0,033	0,243
KEGG_GLIOMA	56	-1,402	0,027	0,251
KEGG_CYTOKINE_CYTOKINE_RECEPTOR_INTERACTION	207	-1,395	0,000	0,254
KEGG_ADHERENS_JUNCTION	63	-1,395	0,037	0,253
KEGG_REGULATION_OF_ACTIN_CYTOSKELETON	185	-1,394	0,011	0,251
REACTOME_CELL_DEATH_SIGNALLING_VIA_NRAGE_NRIF_AND_NADE	52	-1,394	0,026	0,249
KEGG_LEUKOCYTE_TRANSENDOTHELIAL_MIGRATION	95	-1,392	0,013	0,248
REACTOME_GENERIC_TRANSCRIPTION_PATHWAY	122	-1,391	0,007	0,248
KEGG_NEUROTROPHIN_SIGNALING_PATHWAY	112	-1,389	0,007	0,249
PID_BCR_5PATHWAY	62	-1,386	0,024	0,247
KEGG_CHEMOKINE_SIGNALING_PATHWAY	161	-1,382	0,000	0,251

human C2 positive report

GENE SET NAME	SIZE	NES	NOM p-val	FDR q-val
KEGG_RIBOSOME	77	2,820	0,000	0,000
REACTOME_PEPTIDE_CHAIN_ELONGATION	77	2,811	0,000	0,000
REACTOME_SRP_DEPENDENT_COTRANSLATIONAL_PROTEIN_TARGETING_TO_MEMBRANE	98	2,810	0,000	0,000
MIPS_RIBOSOME_CYTOPLASMIC	74	2,802	0,000	0,000
REACTOME_INFLUENZA_VIRAL_RNA_TRANSCRIPTION_AND_REPLICATION	90	2,797	0,000	0,000
REACTOME_3_UTR_MEDIATED_TRANSLATIONAL_REGULATION	84	2,774	0,000	0,000
REACTOME_TRANSLATION	121	2,743	0,000	0,000
MIPS_40S_RIBOSOMAL_SUBUNIT_CYTOPLASMIC	28	2,699	0,000	0,000
REACTOME_FORMATION_OF_THE_TERNARY_COMPLEX_AND_SUBSEQUENTLY_THE_43S_COMPLEX	32	2,689	0,000	0,000
REACTOME_NONSENSE_MEDIATED_DECAY_ENHANCED_BY_THE_EXON_JUNCTION_COMPLEX	90	2,644	0,000	0,000
REACTOME_INFLUENZA_LIFE_CYCLE	121	2,617	0,000	0,000
REACTOME_RESPIRATORY_ELECTRON_TRANSPORT_ATP_SYNTHESIS_BY_CHEMIOSMOTIC_COUPLING_AND_HEAT_PRODUCTION_BY_UNCOUPLING_PROTEINS_	71	2,609	0,000	0,000
REACTOME_ACTIVATION_OF_THE_MRNA_UPON_BINDING_OF_THE_CAP_BINDING_COMPLEX_AND_EIFS_AND_SUBSEQUENT_BINDING_TO_43S	39	2,594	0,000	0,000
REACTOME_RESPIRATORY_ELECTRON_TRANSPORT	55	2,432	0,000	0,000
MIPS_NOP56P_ASSOCIATED_PRE_RRNA_COMPLEX	92	2,396	0,000	0,000
MIPS_60S_RIBOSOMAL_SUBUNIT_CYTOPLASMIC	45	2,356	0,000	0,000
REACTOME_METABOLISM_OF_MRNA	181	2,337	0,000	0,000
REACTOME_TCA_CYCLE_AND_RESPIRATORY_ELECTRON_TRANSPORT	100	2,311	0,000	0,000
KEGG_OXIDATIVE_PHOSPHORYLATION	101	2,265	0,000	0,000
KEGG_PARKINSONS_DISEASE	99	2,245	0,000	0,000
REACTOME_METABOLISM_OF_PROTEINS	322	2,217	0,000	0,000

GENE SET NAME	SIZE	NES	NOM p-val	FDR q-val
REACTOME_METABOLISM_OF_RNA	217	2,195	0,000	0,000
KEGG_HUNTINGTONS_DISEASE	147	1,938	0,000	0,003
KEGG_ALZHEIMERS_DISEASE	139	1,828	0,000	0,014
REACTOME_RNA_POL_II_TRANSCRIPTION_PRE_INITIATION_AND_PROMOTER_OPENING	36	1,811	0,000	0,017
MIPS_55S_RIBOSOME_MITOCHONDRIAL	76	1,800	0,000	0,020
MIPS_TRBP_CONTAINING_COMPLEX_1	22	1,799	0,000	0,019
MIPS_26S_PROTEASOME	22	1,782	0,003	0,024
MIPS_39S_RIBOSOMAL_SUBUNIT_MITOCHONDRIAL	46	1,763	0,001	0,029
BIOCARTA_PROTEASOME_PATHWAY	26	1,758	0,007	0,030
KEGG_PROTEIN_EXPORT	19	1,753	0,004	0,031
KEGG_UBIQUITIN_MEDIATED_PROTEOLYSIS	111	1,731	0,000	0,040
REACTOME_ANTIGEN_PROCESSING_UBIQUITINATION_PROTEASOME_DEGRADATION	161	1,720	0,000	0,044
KEGG_VALINE_LEUCINE_AND_ISOLEUCINE_DEGRADATION	41	1,717	0,001	0,044
KEGG_RNA_DEGRADATION	45	1,688	0,004	0,061
REACTOME_RNA_POL_II_TRANSCRIPTION	80	1,680	0,001	0,064
REACTOME_REGULATION_OF_ORNITHINE_DECARBOXYLASE_ODC	45	1,662	0,003	0,076
REACTOME_VIF_MEDIATED_DEGRADATION_OF_APOBEC3G	45	1,659	0,005	0,076
REACTOME_CLASS_I_MHC_MEDIATED_ANTIGEN_PROCESSING_PRESENTATION	186	1,659	0,000	0,074
REACTOME_MITOCHONDRIAL_PROTEIN_IMPORT	41	1,655	0,008	0,075
REACTOME_RNA_POL_III_TRANSCRIPTION	29	1,623	0,018	0,101
REACTOME_REGULATORY_RNA_PATHWAYS	23	1,613	0,022	0,110
REACTOME_ACTIVATED_AMPK_STIMULATES_FATTY_ACID_OXIDATION_IN_MUSCLE	16	1,601	0,021	0,121
MIPS_PA28_20S_PROTEASOME	16	1,601	0,018	0,119
REACTOME_BRANCHED_CHAIN_AMINO_ACID_CATABOLISM	16	1,593	0,022	0,125
REACTOME_DEADENYLATION_DEPENDENT_MRNA_DECAY	36	1,591	0,016	0,125
REACTOME_MRNA_SPLICING_MINOR_PATHWAY	29	1,589	0,017	0,124
REACTOME_MICRORNA_MIRNA_BIOGENESIS	20	1,582	0,019	0,131
MIPS_PA700_20S_PA28_COMPLEX	34	1,578	0,012	0,134
REACTOME_RNA_POL_III_TRANSCRIPTION_INITIATION_FROM_TYPE_3_PROMOTER	23	1,570	0,015	0,142
KEGG_PROTEASOME	40	1,566	0,017	0,144
REACTOME_RNA_POL_III_TRANSCRIPTION_TERMINATION	17	1,566	0,026	0,142
MIPS_RNA_POLYMERASE_II	16	1,558	0,031	0,149
KEGG_RETINOL_METABOLISM	24	1,555	0,032	0,151
REACTOME_CROSS_PRESENTATION_OF_SOLUBLE_EXOGENOUS_ANTIGENS_ENDOSOMES	43	1,554	0,010	0,150
MIPS_RNA_POLYMERASE_II_HOLOENZYME_COMPLEX	23	1,547	0,027	0,157
REACTOME_RNA_POL_II_PRE_TRANSCRIPTION_EVENTS	52	1,543	0,011	0,159
KEGG_PROPANOATE_METABOLISM	27	1,542	0,022	0,158
REACTOME_DESTABILIZATION_OF_MRNA_BY_AUF1_HNRNP_D0	45	1,533	0,013	0,168
MIPS_LARGE_DROSHA_COMPLEX	15	1,530	0,026	0,169
REACTOME_MRNA_SPLICING	65	1,527	0,021	0,171
REACTOME_RNA_POL_III_CHAIN_ELONGATION	15	1,524	0,043	0,172
REACTOME_APOPTOTIC_CLEAVAGE_OF_CELLULAR_PROTEINS	32	1,520	0,034	0,176
BIOCARTA_IGF1MTOR_PATHWAY	17	1,515	0,036	0,180
KEGG_RNA_POLYMERASE	24	1,513	0,036	0,181
BIOCARTA_CK1_PATHWAY	16	1,512	0,033	0,179
REACTOME_RNA_POL_III_TRANSCRIPTION_INITIATION_FROM_TYPE_2_PROMOTER	20	1,509	0,039	0,181
REACTOME_ER_PHAGOSOME_PATHWAY	49	1,506	0,024	0,184
REACTOME_ENOS_ACTIVATION_AND_REGULATION	17	1,504	0,030	0,183
PID_FOXOPATHWAY	43	1,488	0,029	0,207
KEGG_PYRIMIDINE_METABOLISM	85	1,487	0,015	0,205

GENE SET NAME	SIZE	NES	NOM p-val	FDR q-val
MIPS_17S_U2_SNRNP	27	1,484	0,039	0,208
REACTOME_SCF_BETA_TRCP_MEDIATED_DEGRADATION_OF_EMI1	45	1,478	0,031	0,215
REACTOME_ANTIGEN_PROCESSING_CROSS_PRESENTATION	61	1,478	0,029	0,213
KEGG_CARDIAC_MUSCLE_CONTRACTION	65	1,477	0,021	0,212
REACTOME_TRAFFICKING_OF_AMPA_RECEPTORS	19	1,462	0,047	0,231
REACTOME_CDT1_ASSOCIATION_WITH_THE_CDC6_ORC_ORIGIN_COMPLEX	44	1,460	0,026	0,232
REACTOME_MRNA_CAPPING	26	1,460	0,027	0,230
REACTOME_AUTODEGRADATION_OF_CDH1_BY_CDH1_APC_C	53	1,458	0,031	0,230
REACTOME_APOPTOTIC_EXECUTION_PHASE	45	1,451	0,029	0,237
PID_P53REGULATIONPATHWAY	50	1,441	0,038	0,249

mouse C2 negative report

GENE SET NAME	SIZE	NES	NOM p-val	FDR q-val
GALINDO_IMMUNE_RESPONSE_TO_ENTEROTOXIN	71	-2,362	0,000	0,003
QI_PLASMACYTOMA_UP	241	-2,095	0,000	0,012
ALTEMEIER_RESPONSE_TO_LPS_WITH_MECHANICAL_VENTILATION	101	-2,011	0,000	0,021
SHIN_B_CELL_LYMPHOMA_CLUSTER_8	35	-1,957	0,000	0,029
BROWN_MYELOID_CELL_DEVELOPMENT_UP	121	-1,949	0,000	0,026
ICHIBA_GRAFT_VERSUS_HOST_DISEASE_D7_UP	84	-1,909	0,000	0,034
ICHIBA_GRAFT_VERSUS_HOST_DISEASE_35D_UP	107	-1,883	0,000	0,038
MARKEY_RB1_ACUTE_LOF_UP	168	-1,876	0,000	0,035
LI_INDUCED_T_TO_NATURAL_KILLER_UP	213	-1,838	0,000	0,044
WUNDER_INFLAMMATORY_RESPONSE_AND_CHOLESTEROL_UP	37	-1,825	0,004	0,044
HESS_TARGETS_OF_HOXA9_AND_MEIS1_DN	64	-1,735	0,000	0,082
NADLER_OBESITY_UP	54	-1,715	0,004	0,089
NEMETH_INFLAMMATORY_RESPONSE_LPS_UP	72	-1,682	0,005	0,104
STEARMAN_TUMOR_FIELD_EFFECT_UP	28	-1,665	0,010	0,110
VILIMAS_NOTCH1_TARGETS_UP	49	-1,654	0,004	0,112
KHETCHOUMIAN_TRIM24_TARGETS_UP	44	-1,638	0,000	0,117
STEARMAN_LUNG_CANCER_EARLY_VS_LATE_DN	46	-1,627	0,005	0,119
CLASPER_LYMPHATIC_VESSELS_DURING_METASTASIS_UP	19	-1,626	0,021	0,113
VILIMAS_NOTCH1_TARGETS_DN	18	-1,612	0,024	0,118
FUKUSHIMA_TNFSF11_TARGETS	15	-1,587	0,025	0,132
SEKI_INFLAMMATORY_RESPONSE_LPS_UP	65	-1,565	0,000	0,149
MORI_IMMATURE_B_LYMPHOCYTE_UP	41	-1,557	0,020	0,150
QI_HYPOXIA_TARGETS_OF_HIF1A_AND_FOXA2	28	-1,540	0,043	0,162
WORSCHECH_TUMOR_EVASION_AND_TOLEROGENICITY_UP	29	-1,532	0,035	0,164
SHIN_B_CELL_LYMPHOMA_CLUSTER_3	26	-1,530	0,037	0,159
SHIN_B_CELL_LYMPHOMA_CLUSTER_5	16	-1,523	0,045	0,155
MARTORIATI_MDM4_TARGETS_FETAL_LIVER_UP	144	-1,523	0,000	0,150
LIAN_LIPA_TARGETS_3M	52	-1,518	0,018	0,151
LEE_AGING_CEREBELLUM_UP	74	-1,518	0,006	0,146
ZHANG_TLX_TARGETS_36HR_UP	171	-1,496	0,000	0,163
JIANG_AGING_HYPOTHALAMUS_DN	38	-1,487	0,020	0,170
BILANGES_SERUM_SENSITIVE_GENES	69	-1,439	0,000	0,225
LIAN_LIPA_TARGETS_6M	65	-1,437	0,032	0,222
HOFFMANN_SMALL_PRE_BII_TO_IMMATURE_B_LYMPHOCYTE_UP	52	-1,423	0,034	0,234
KASLER_HDAC7_TARGETS_1_UP	142	-1,415	0,000	0,241

mouse C2 positive report

GENE SET NAME	SIZE	NES	NOM p-val	FDR q-val
BILANGES_SERUM_AND_RAPAMYCIN_SENSITIVE_GENES	59	2,515	0,000	0,000
MODY_HIPPOCAMPUS_PRENATAL	36	2,182	0,000	0,000
MILI_PSEUDOPODIA_HAPTOTAXIS_UP	332	2,146	0,000	0,000
SCHAEFFER_PROSTATE_DEVELOPMENT_6HR_UP	125	2,043	0,000	0,002
YAO_TEMPORAL_RESPONSE_TO_PROGESTERONE_CLUSTER_13	126	1,960	0,000	0,005
WANG_LSD1_TARGETS_UP	20	1,950	0,000	0,005
ZHANG_BREAST_CANCER_PROGENITORS_UP	281	1,892	0,000	0,015
LANDIS_ERBB2_BREAST_TUMORS_324_DN	125	1,890	0,000	0,013
SCHAEFFER_PROSTATE_DEVELOPMENT_AND_CANCER_BOX4_DN	23	1,876	0,000	0,015
BURTON_ADIPOGENESIS_11	42	1,827	0,000	0,024
STEARMAN_LUNG_CANCER_EARLY_VS_LATE_UP	86	1,823	0,000	0,023
YAO_TEMPORAL_RESPONSE_TO_PROGESTERONE_CLUSTER_10	43	1,813	0,000	0,024
BURTON_ADIPOGENESIS_5	90	1,770	0,000	0,040
WANG_TUMOR_INVASIVENESS_UP	288	1,751	0,000	0,049
BURTON_ADIPOGENESIS_12	21	1,749	0,004	0,047
LANDIS_ERBB2_BREAST_PRENEOPLASTIC_DN	48	1,732	0,000	0,055
LANDIS_BREAST_CANCER_PROGRESSION_DN	62	1,732	0,001	0,052
STARK_PREFRONTAL_CORTEX_22Q11_DELETION_DN	338	1,726	0,000	0,053
JIANG_AGING_HYPOTHALAMUS_UP	39	1,723	0,000	0,052
MILI_PSEUDOPODIA_CHEMOTAXIS_UP	39	1,710	0,001	0,057
LANDIS_ERBB2_BREAST_TUMORS_65_DN	30	1,704	0,004	0,059
GOLDRATH_HOMEOSTATIC_PROLIFERATION	123	1,704	0,001	0,056
PLASARI_TGFB1_TARGETS_10HR_DN	193	1,696	0,000	0,059
ZHANG_TLX_TARGETS_36HR_DN	122	1,688	0,001	0,063
ELLWOOD_MYC_TARGETS_DN	26	1,686	0,008	0,062
BOUDOUKHA_BOUND_BY_IGF2BP2	82	1,685	0,000	0,059
PLASARI_NFIC_TARGETS_BASAL_DN	17	1,685	0,010	0,058
IKEDA_MIR30_TARGETS_UP	107	1,684	0,000	0,056
MCBRYAN_PUBERTAL_BREAST_5_6WK_UP	84	1,681	0,000	0,056
CUI_TCF21_TARGETS_UP	32	1,673	0,009	0,059
BURTON_ADIPOGENESIS_6	145	1,655	0,000	0,070
JIANG_AGING_CEREBRAL_CORTEX_UP	32	1,614	0,007	0,108
ZHENG_FOXP3_TARGETS_IN_THYMUS_UP	133	1,607	0,000	0,112
CADWELL_ATG16L1_TARGETS_UP	68	1,601	0,004	0,115
CHIARADONNA_NEOPLASTIC_TRANSFORMATION_CDC25_UP	98	1,593	0,002	0,122
PAL_PRMT5_TARGETS_UP	160	1,591	0,001	0,121
SHETH_LIVER_CANCER_VS_TXNIP_LOSS_PAM4	200	1,578	0,000	0,135
HOWLIN_PUBERTAL_MAMMARY_GLAND	59	1,578	0,005	0,132
PLASARI_TGFB1_SIGNALING_VIA_NFIC_10HR_UP	42	1,571	0,007	0,137
BILANGES_RAPAMYCIN_SENSITIVE_VIA_TSC1_AND_TSC2	52	1,559	0,010	0,151
WAKABAYASHI_ADIPOGENESIS_PPARG_RXRA_BOUND_WITH_H4K20ME1_MARK	95	1,558	0,002	0,147
MCBRYAN_PUBERTAL_BREAST_4_5WK_UP	209	1,555	0,001	0,148
MORI_SMALL_PRE_BII_LYMPHOCYTE_UP	68	1,553	0,011	0,147
KARLSSON_TGFB1_TARGETS_DN	156	1,548	0,001	0,150
RUAN_RESPONSE_TO_TNF_DN	74	1,545	0,009	0,151
TORCHIA_TARGETS_OF_EWSR1_FLI1_FUSION_TOP20_UP	17	1,520	0,043	0,188
SWEET_LUNG_CANCER_KRAS_DN	367	1,517	0,000	0,191
CUI_TCF21_TARGETS_2_UP	299	1,516	0,000	0,189
IGLESIAS_E2F_TARGETS_UP	129	1,505	0,002	0,201
HANSON_HRAS_SIGNALING_VIA_NFKB	18	1,504	0,043	0,199
YAUCH_HEDGEHOG_SIGNALING_PARACRINE_DN	175	1,504	0,003	0,196

GENE SET NAME	SIZE	NES	NOM p-val	FDR q-val
PILON_KLF1_TARGETS_UP	365	1,499	0,000	0,202
MARTINEZ_TP53_TARGETS_UP	459	1,498	0,000	0,198
CHESLER_BRAIN_HIGHEST_EXPRESSION	30	1,493	0,044	0,205
NADLER_OBESITY_DN	44	1,493	0,029	0,201
BILANGES_SERUM_RESPONSE_TRANSLATION	30	1,491	0,029	0,202
MARTORIATI_MDM4_TARGETS_FETAL_LIVER_DN	395	1,488	0,000	0,203
LANDIS_ERBB2_BREAST_TUMORS_65_UP	18	1,484	0,049	0,206
BERENJENO_TRANSFORMED_BY_RHOA_FOREVER_DN	27	1,483	0,049	0,204
YU_MYC_TARGETS_UP	34	1,479	0,031	0,209
MARKEY_RB1_ACUTE_LOF_DN	178	1,477	0,001	0,209
WANG_TARGETS_OF_MLL_CBP_FUSION_DN	34	1,477	0,043	0,206
WANG_CLASSIC_ADIPOGENIC_TARGETS_OF_PPARG	24	1,477	0,039	0,203
MARTINEZ_RB1_AND_TP53_TARGETS_UP	465	1,455	0,001	0,230
RAMALHO_STEMNESS_UP	157	1,455	0,008	0,227
IVANOVA_HEMATOPOIESIS_STEM_CELL_SHORT_TERM	18	1,453	0,048	0,228